The Abdus Salam
International Centre for Theoretical Physics

United Nations
Educational, Scientific and
Cultural Organization

IAEA
International Atomic Energy Agency

SMR/1843-3

X-Ray Emission Techniques for Forensic Applications

28 May - 1 June, 2007

X-ray Tube-Based Micro-Analytical Techniques at the IAEA Laboratories in Seibersdorf

Dariusz Wegrzynek
IAEA, Vienna

X-ray Tube-Based Micro-Analytical Techniques at the IAEA Laboratories in Seibersdorf

Dariusz Wegrzynek

IAEA

International Atomic Energy Agency

Outline

- Our laboratory
- What are the micro-analytical techniques at our disposal
- Micro-beam X-ray spectrometry – focusing X-rays
- Our X-ray tube based micro-beam spectrometer
- Applications
- Synchrotron is better than X-ray tube
- Conclusions
- Acknowledgement

IAEA

IAEA Seibersdorf Laboratories

The IAEA Laboratories are located about 35 km south of Vienna, Austria

IAEA

X-Ray Fluorescence Group

- The XRF Group is part of the Instrumentation Unit which belongs to Physics, Chemistry, Instrumentation (PCI) Laboratory.
- It is a small team of 3 persons.
- Main activities include support to the IAEA Technical Cooperation Projects, training of the Agency's fellows, provision of in-house analytical services, development of equipment and software for selected applications.

IAEA

Micro-Analytical X-Ray Techniques

Two types of micro-analytical X-ray tube based techniques available:

- total reflection X-ray fluorescence spectrometry
- micro-beam, scanning X-ray fluorescence and absorption spectrometry

IAEA

Focusing X-ray radiation

In a similar fashion like visible light, X-rays are refracted and reflected at an interface between two media.

$$n_{X-rays} < 1 \quad whereas \quad n_{visible\ light} > 1$$

The “inverted” picture of the phenomenon for X-rays as compared to the picture for visible light is due to distinct values of the refractive index for X-rays and visible light in e.g. glass.

IAEA

Refraction and reflection

- for visible light:
  medium 1 – glass,
  medium 2 – air,
  n_1 = 1.5, n_2 = 1
- for 17.5keV X-rays:
  medium 1 – air,
  medium 2 – glass,
  n_1 = 1,
  n_2 = 0.9999985

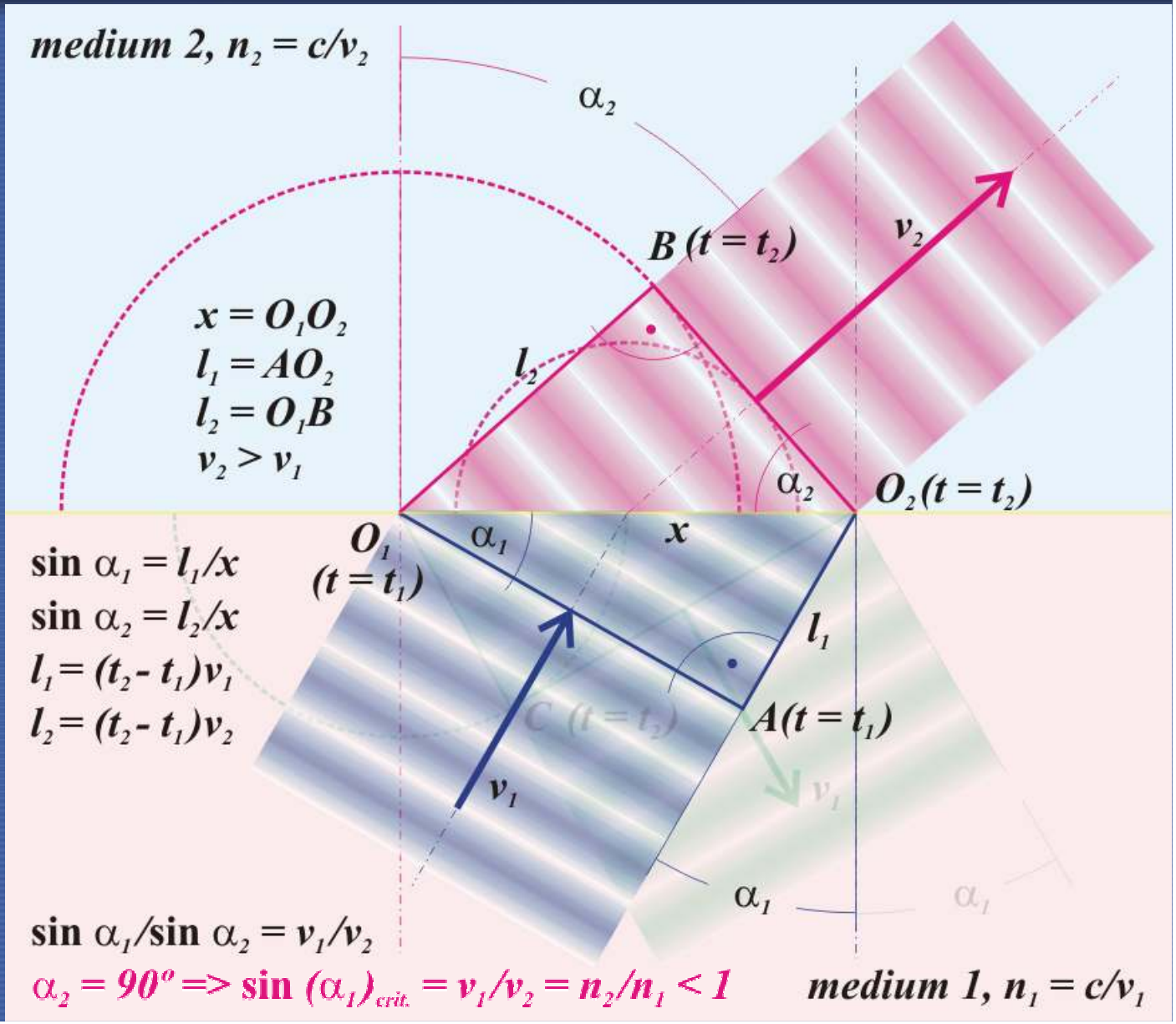

IAEA

Total internal (light) and external (X-rays) reflection

- for visible light:
  medium 1 – glass,
  medium 2 – air,
  $(\alpha_1)_{crit.} \approx 49^o$
- for 17.5keV X-rays:
  medium 1 – air,
  medium 2 – glass,
  $(\alpha_1)_{crit.} \approx 89.9^o$

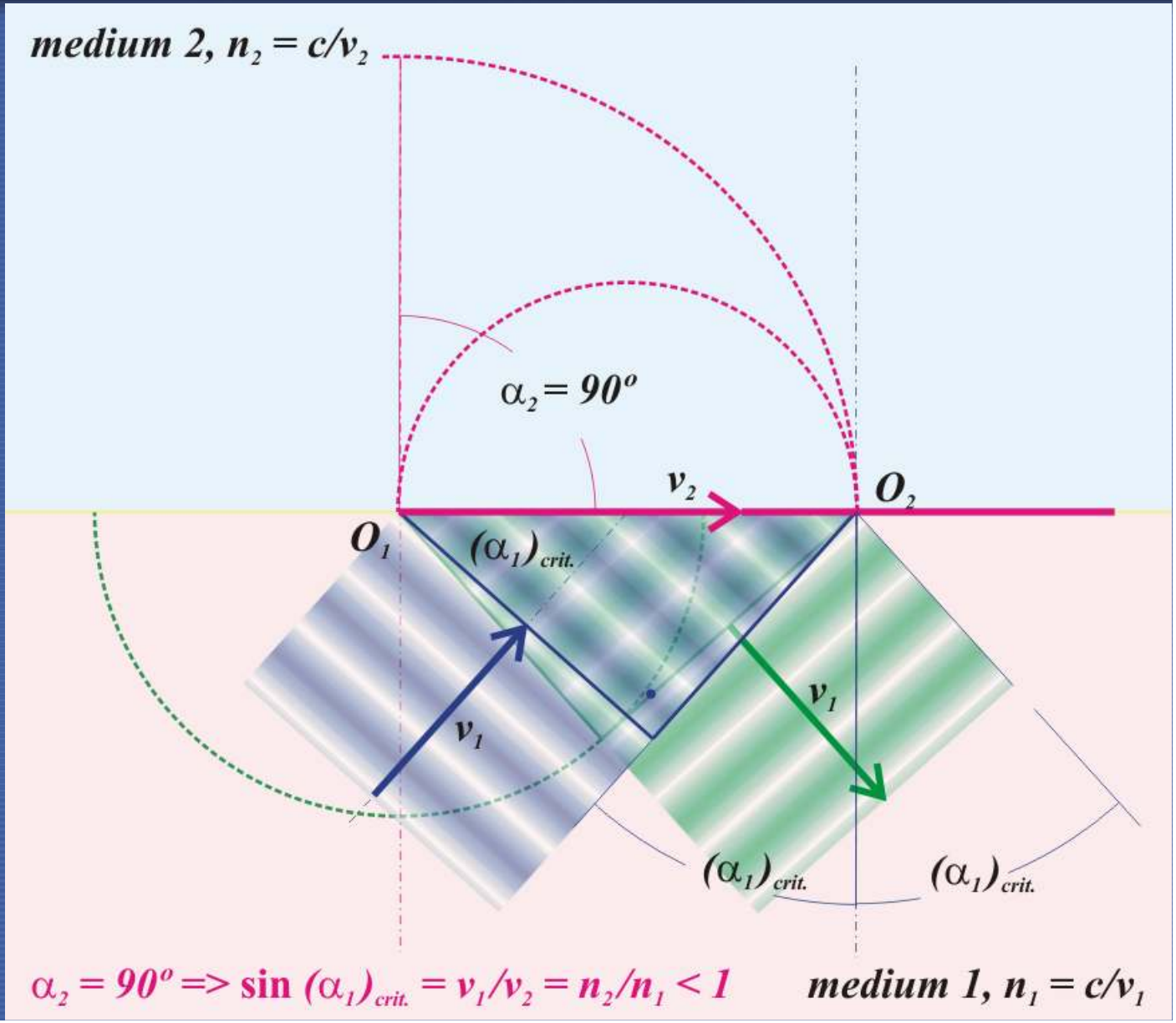

IAEA

X-ray fluorescence and absorption mapping

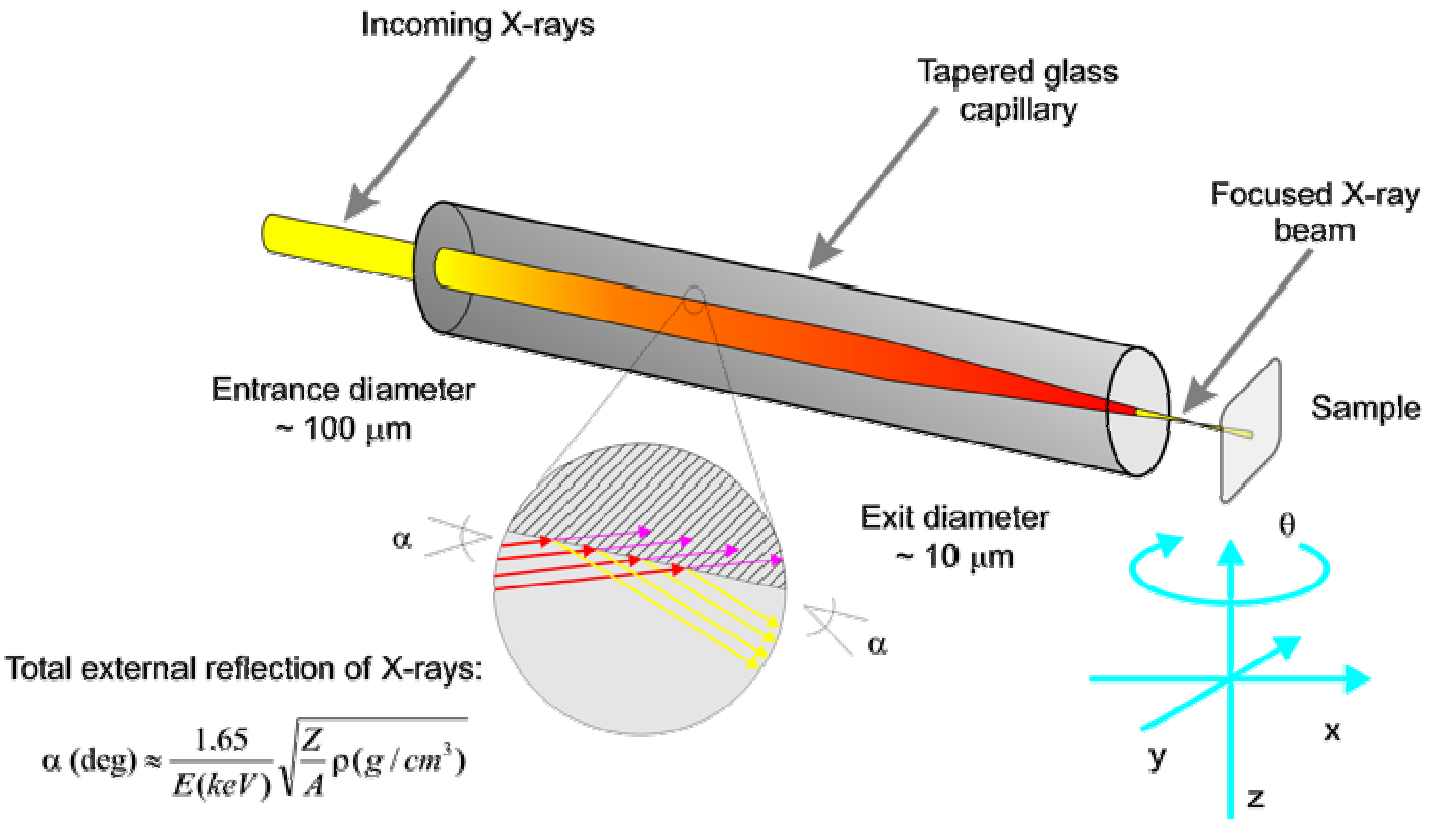

Total external reflection of X-rays:

$$\alpha\,(\mathrm{deg}) \approx \frac{1.65}{E(keV)}\sqrt{\frac{Z}{A}\rho(g/cm^3)}$$

X-ray confocal microscopy

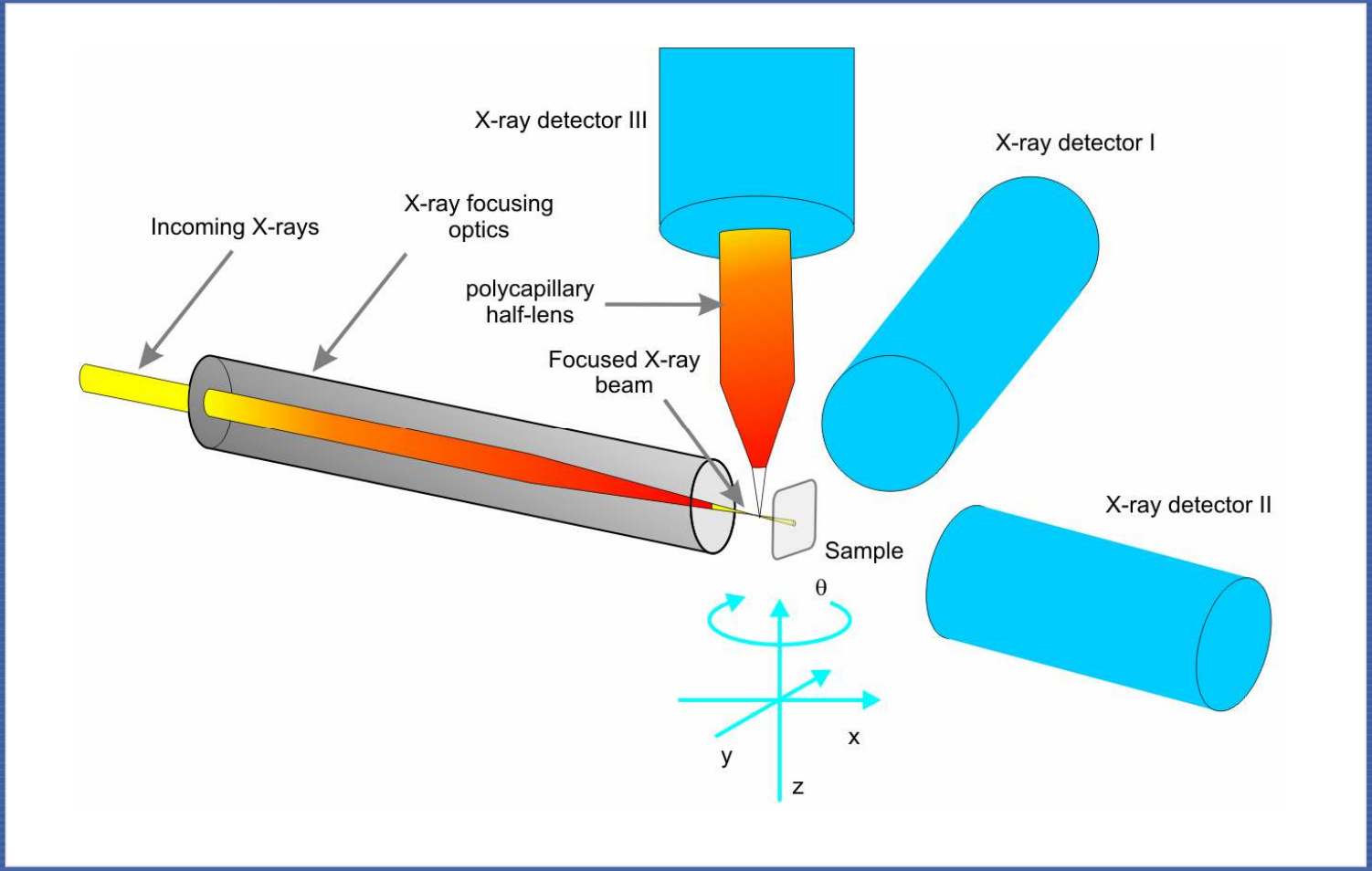

X-ray focusing optics

Polycapillary lens

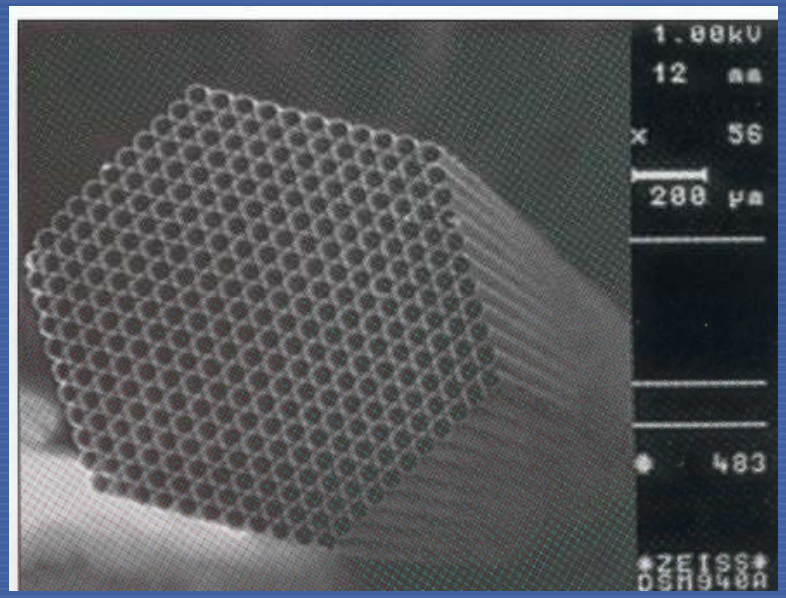

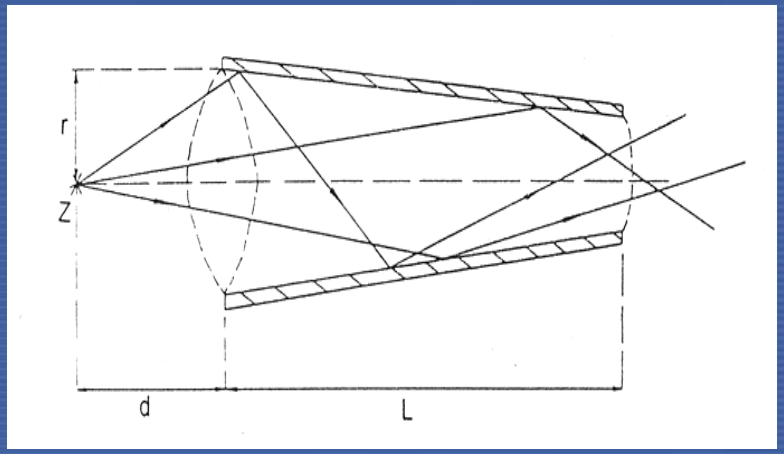

IAEA

X-ray focusing optics

Refractive lens

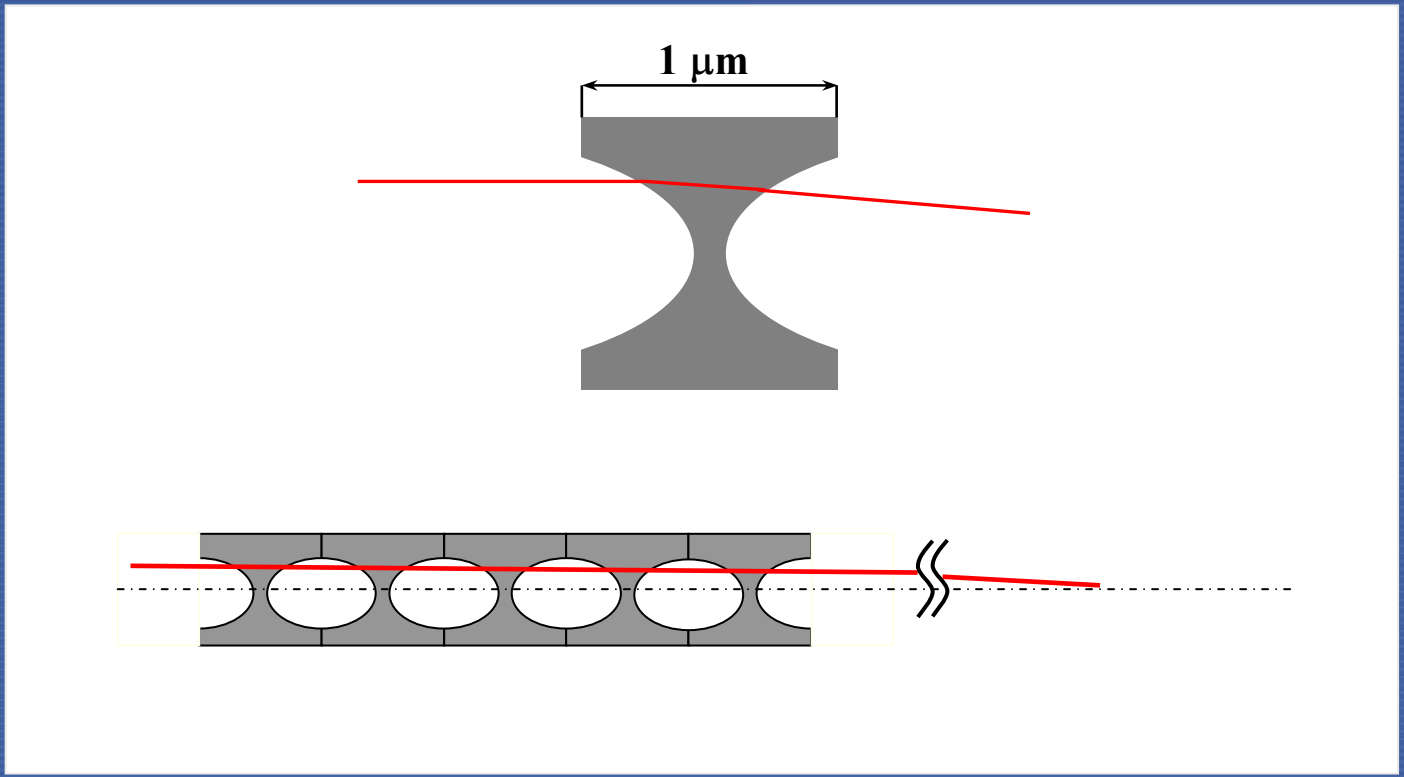

Micro-beam X-ray Setup Scheme

spatial resolution:
15 - 40 μm

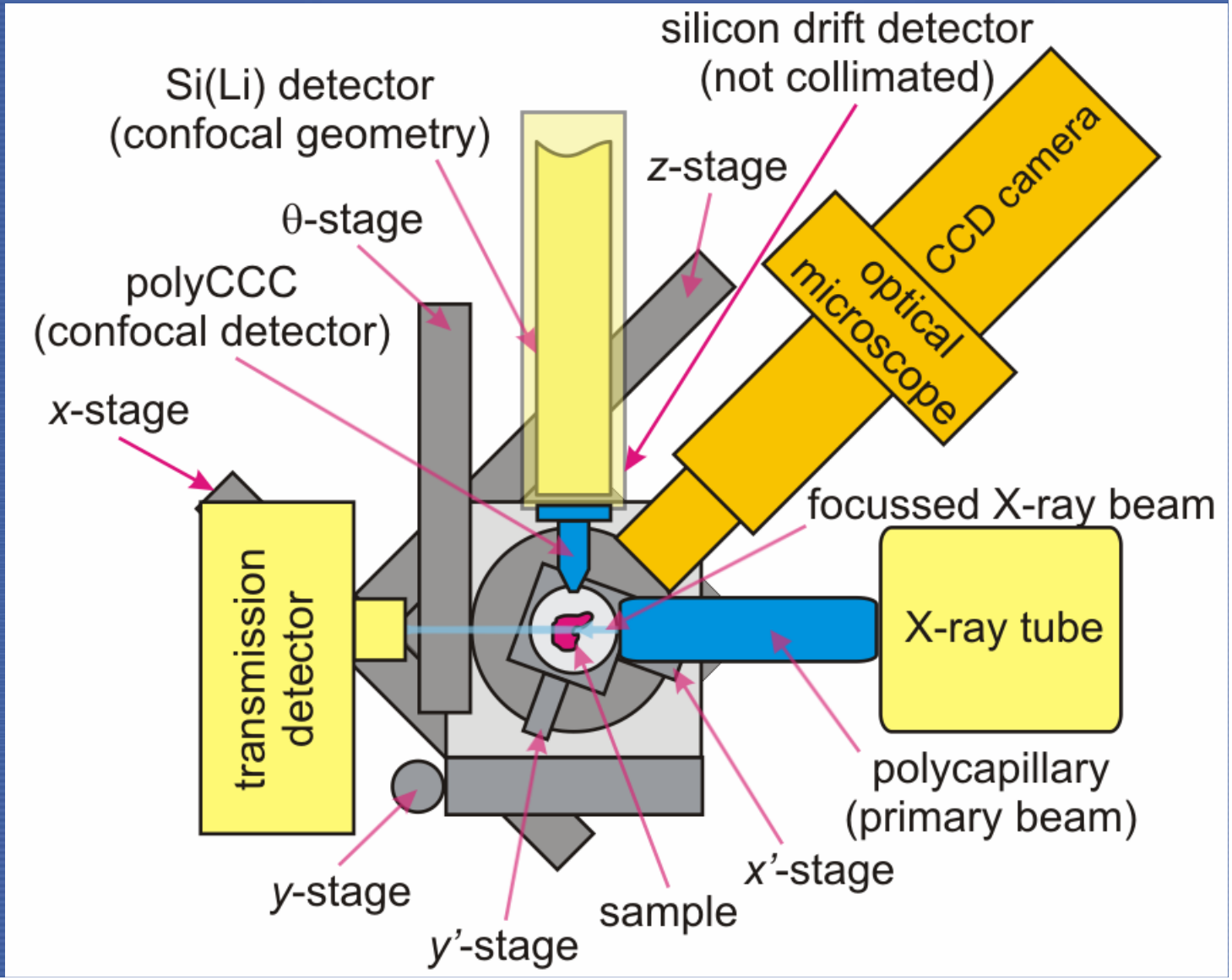

IAEA

The Micro-Beam X-ray Scanning Spectrometer

Si drift detector (fluorescence) on a stage

optical microscope

X-ray tube

Si(Li) detector (confocal)

transmission detector stage

sample stage

optical bench

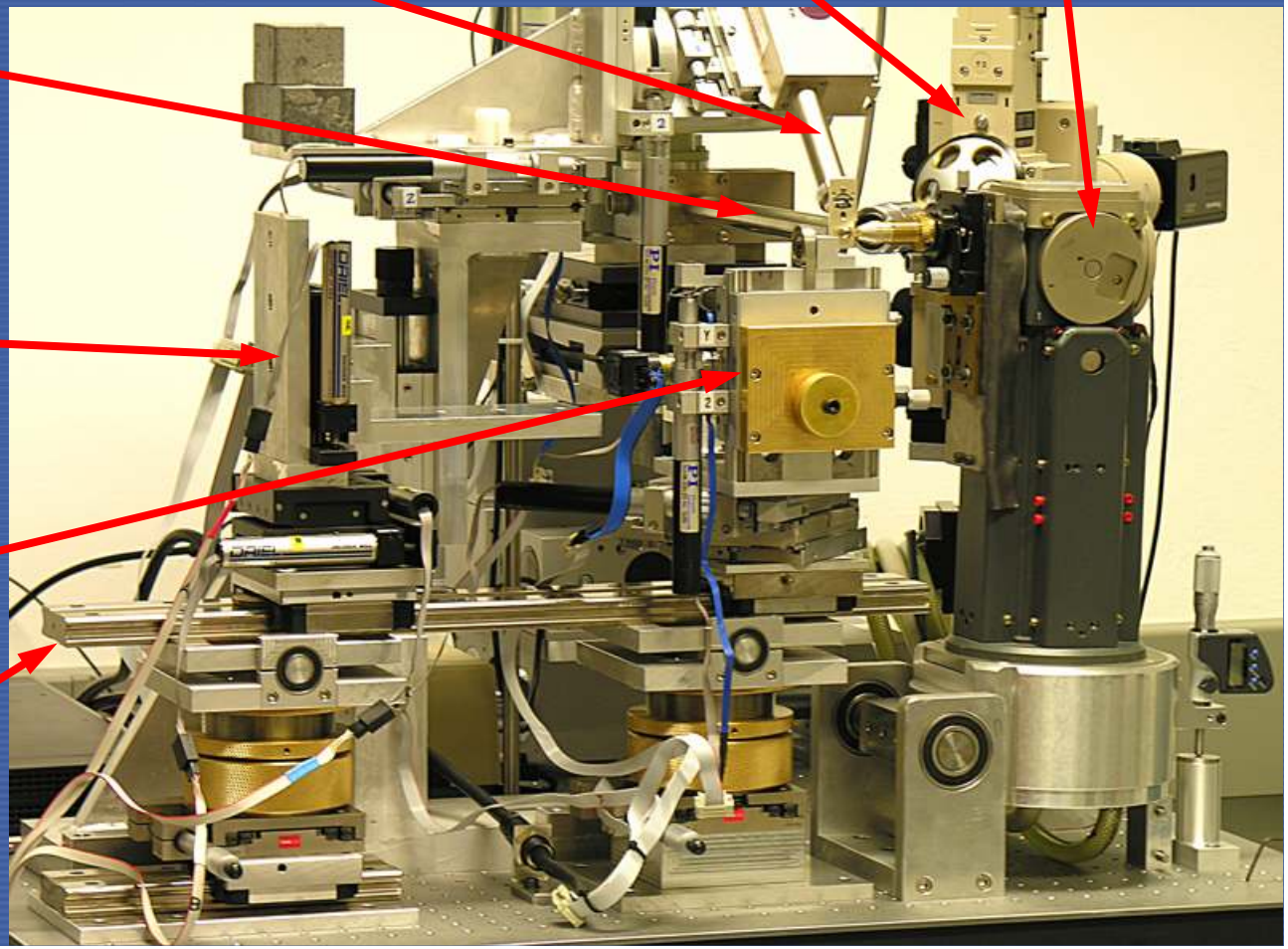

IAEA

Measuring geometry

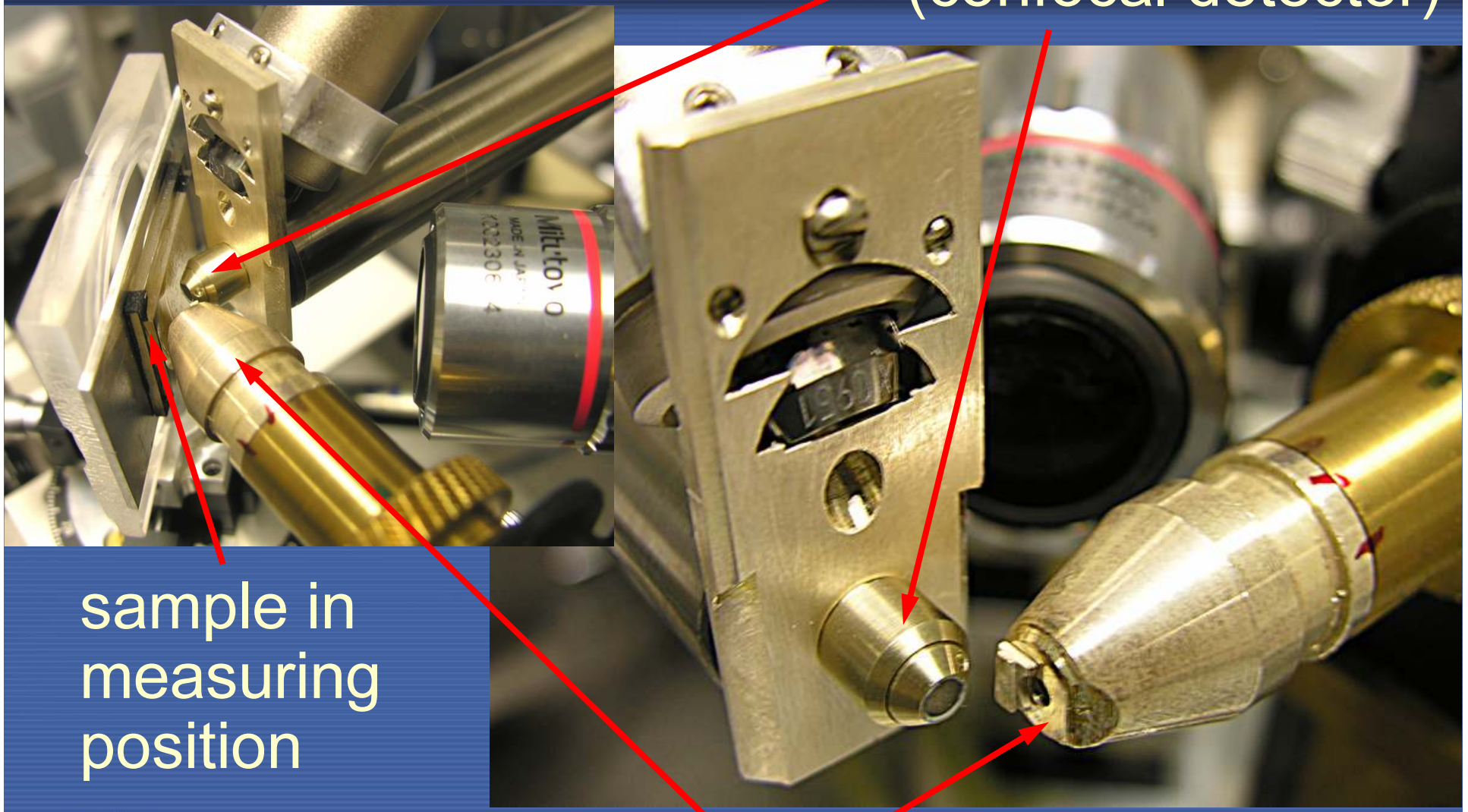

IAEA

Detection Limits of Elements

40 μm
t = 1000s

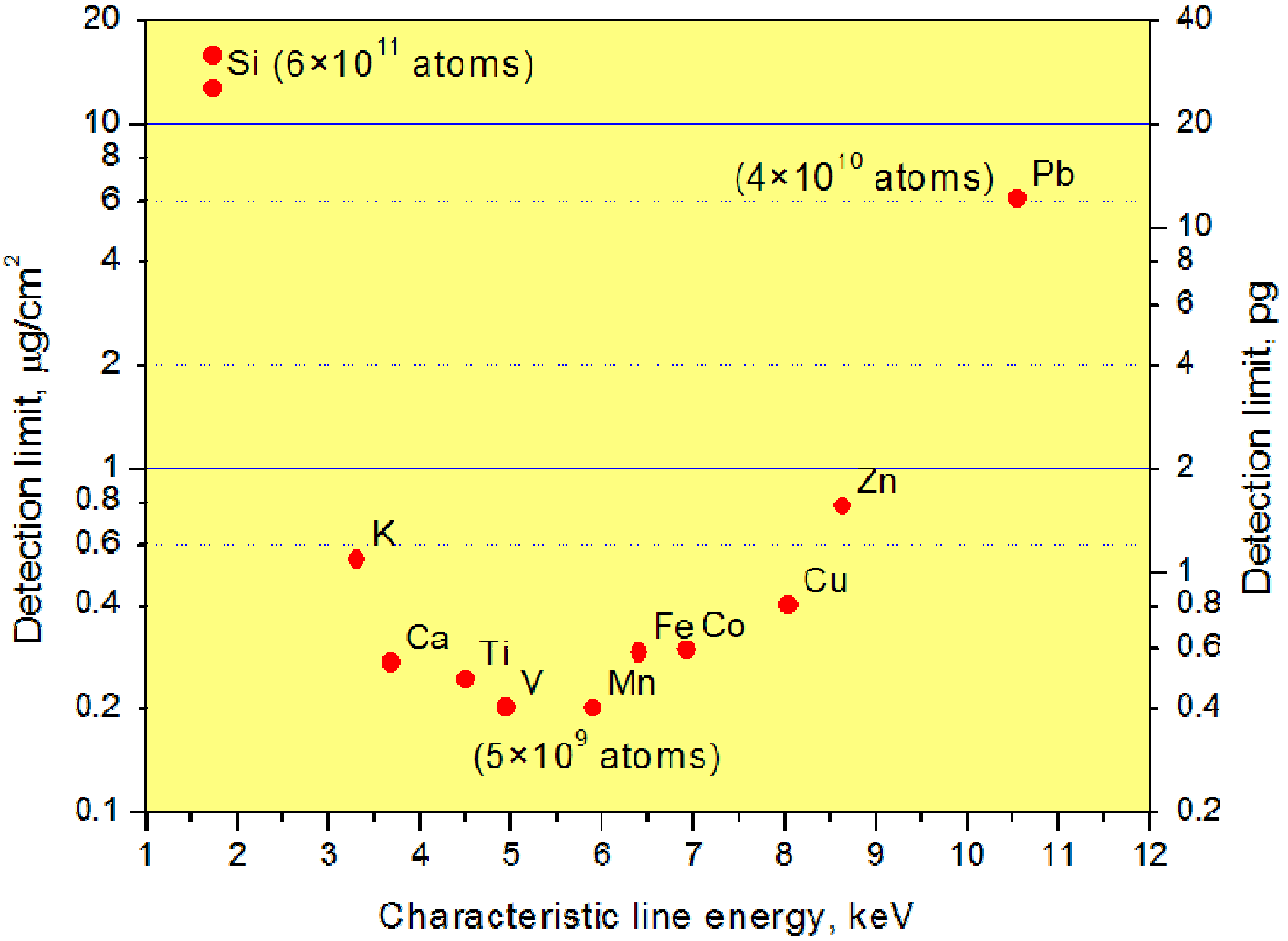

IAEA

Data acquisition software

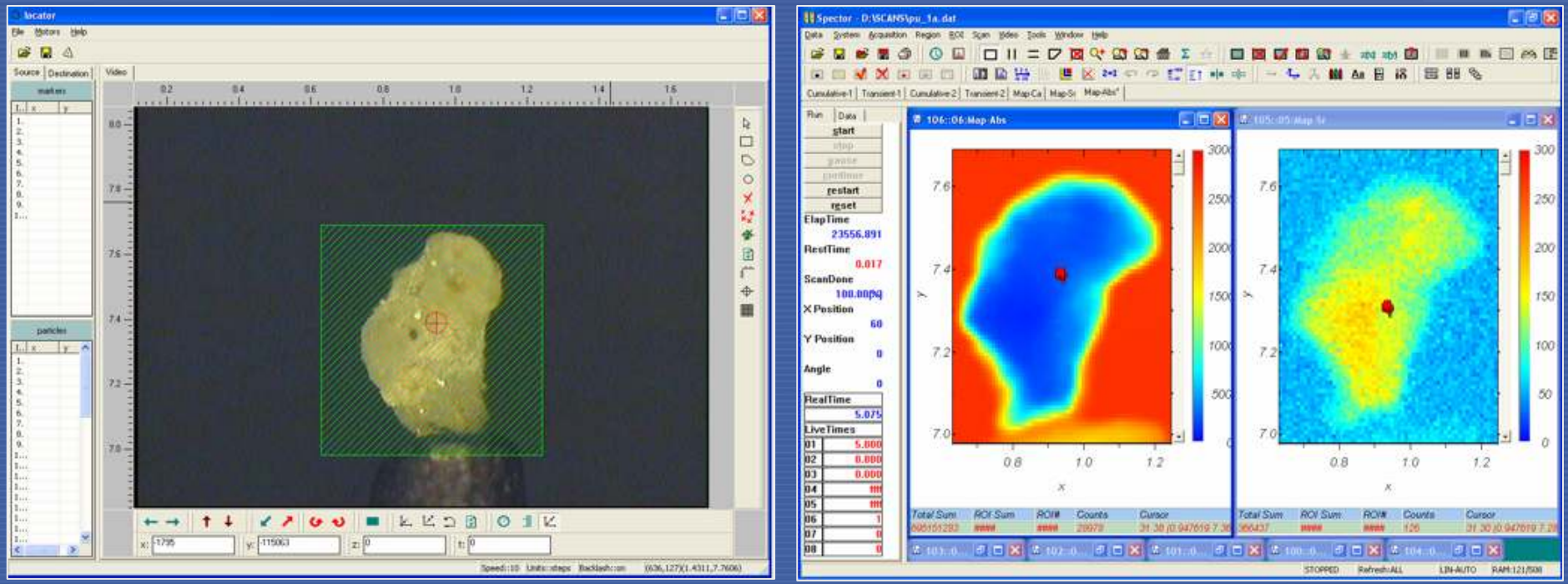

SPECTOR-LOCATOR: microscopic image of the sample (×150) and the collected X-ray absorption/fluorescence images

Detection of U-rich particles in contaminated soil

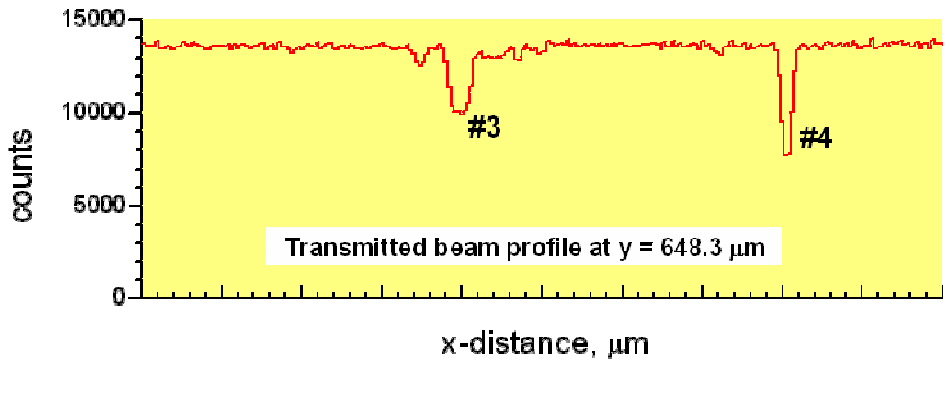

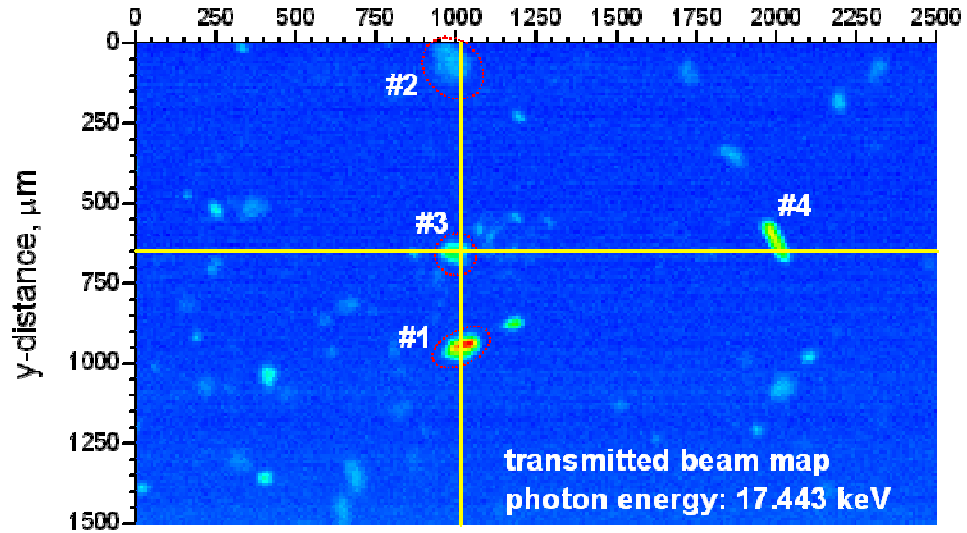

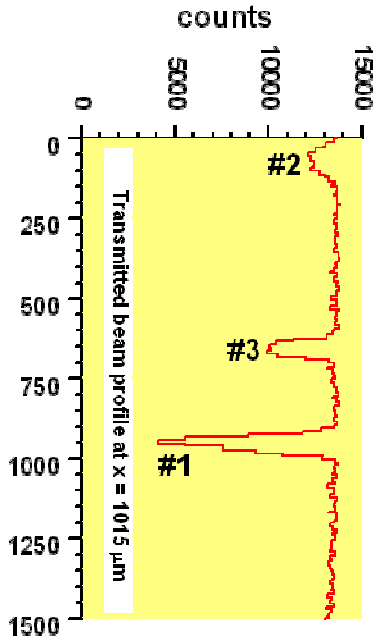

IAEA

Detection of U-rich particles in contaminated soil

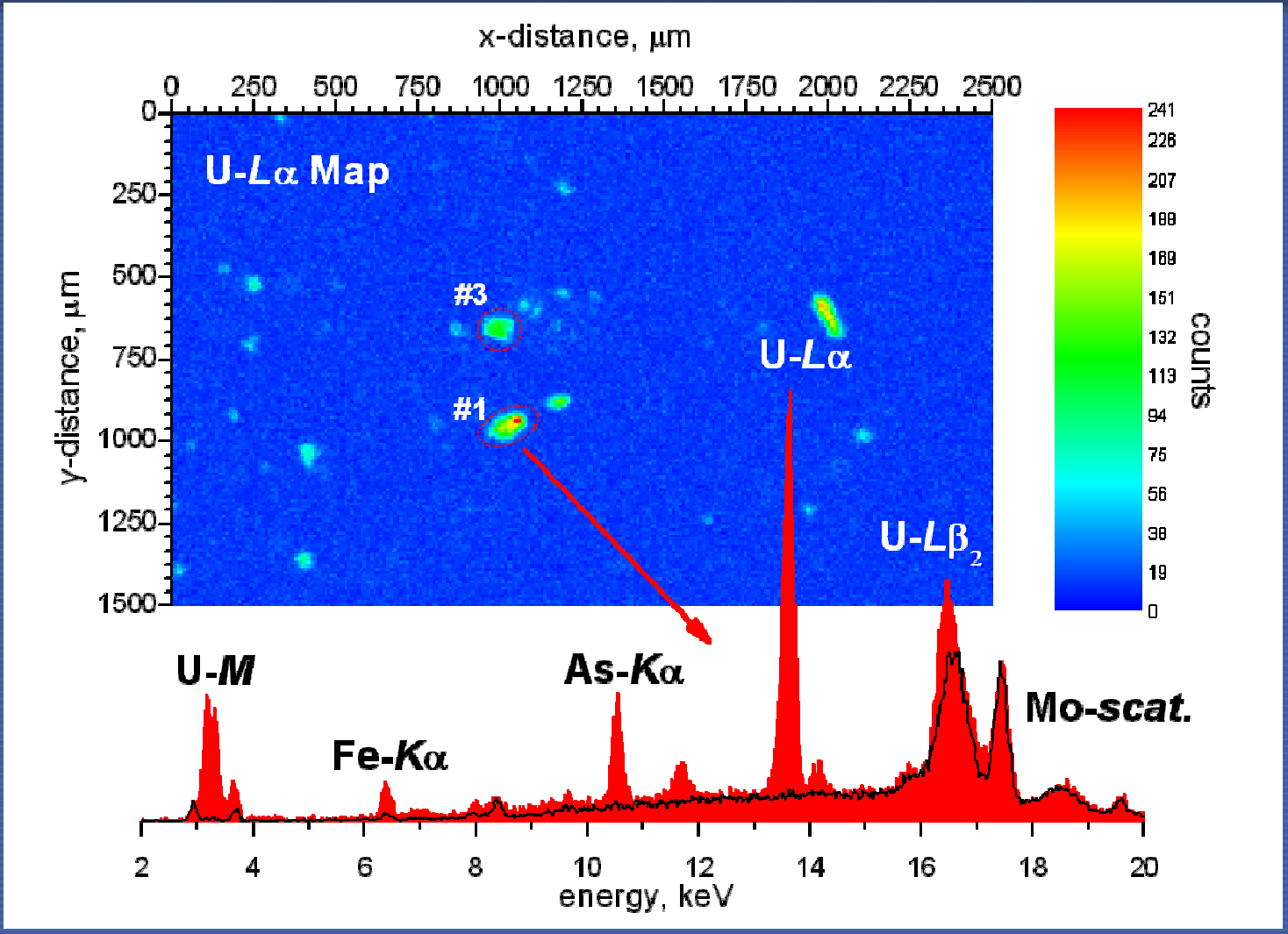

IAEA

Detection of U-rich particles in contaminated soil

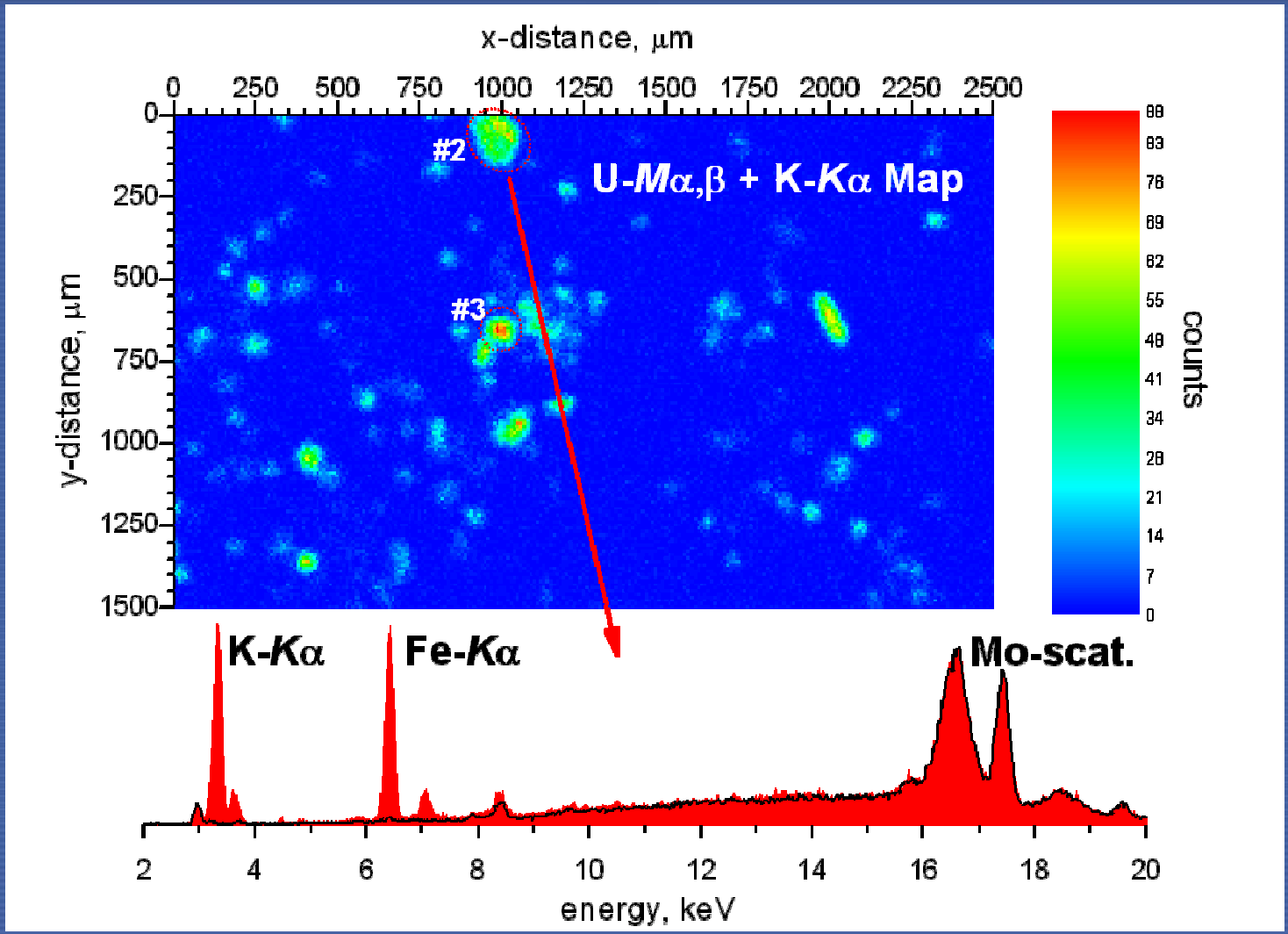

IAEA

Detection of U-rich particles in contaminated soil

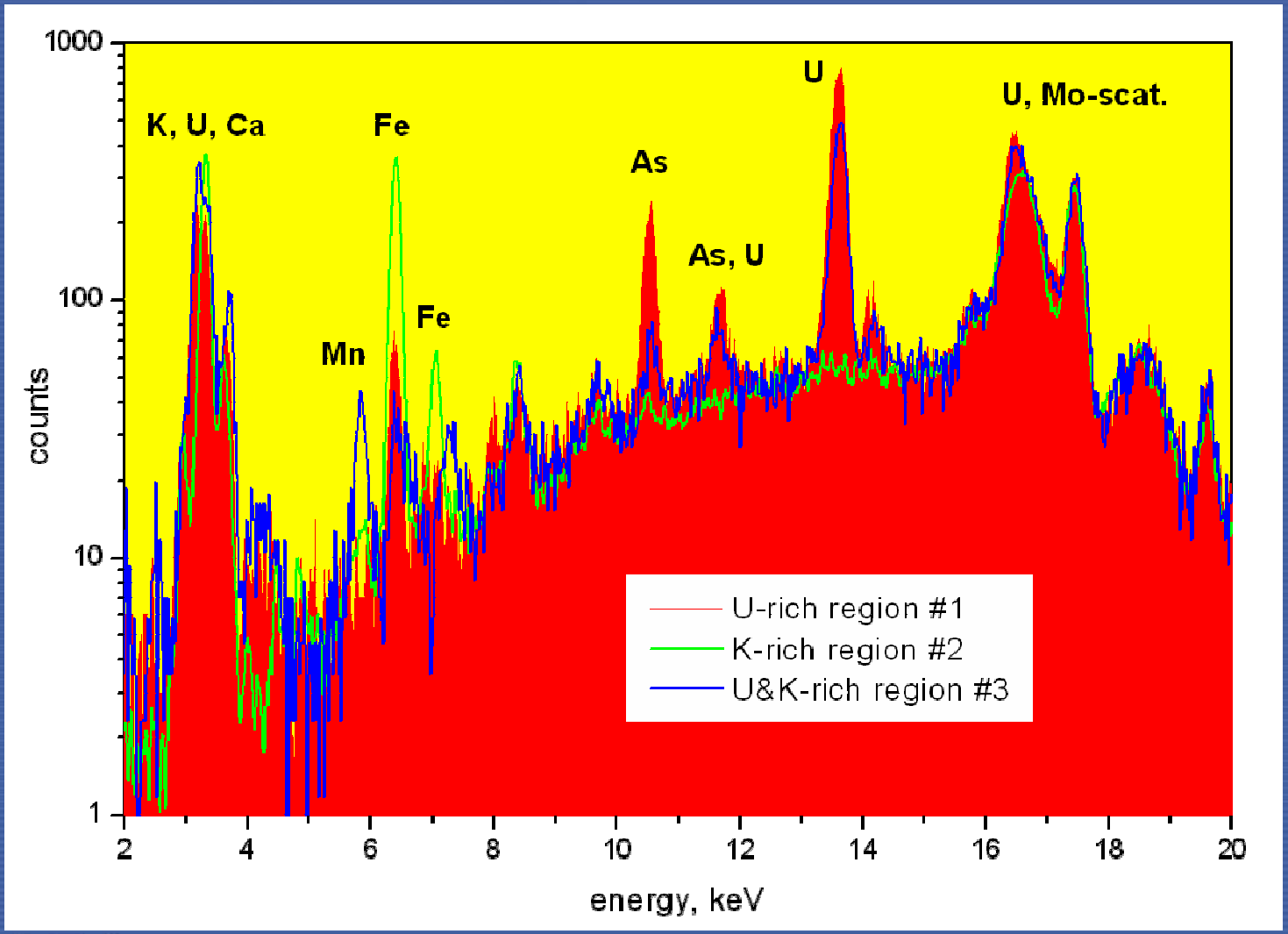

IAEA

Identification of minerals

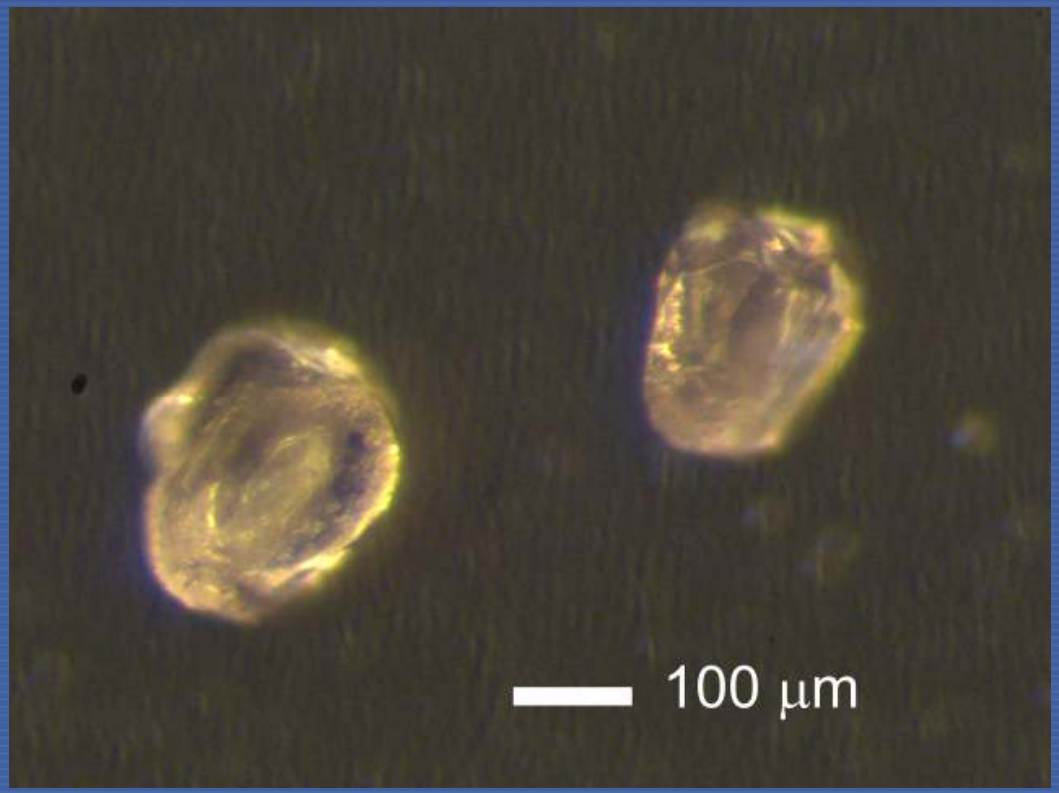

Two “similar” garnets: almandine-spessartine (left) and almandine (right)

IAEA

Identification of minerals

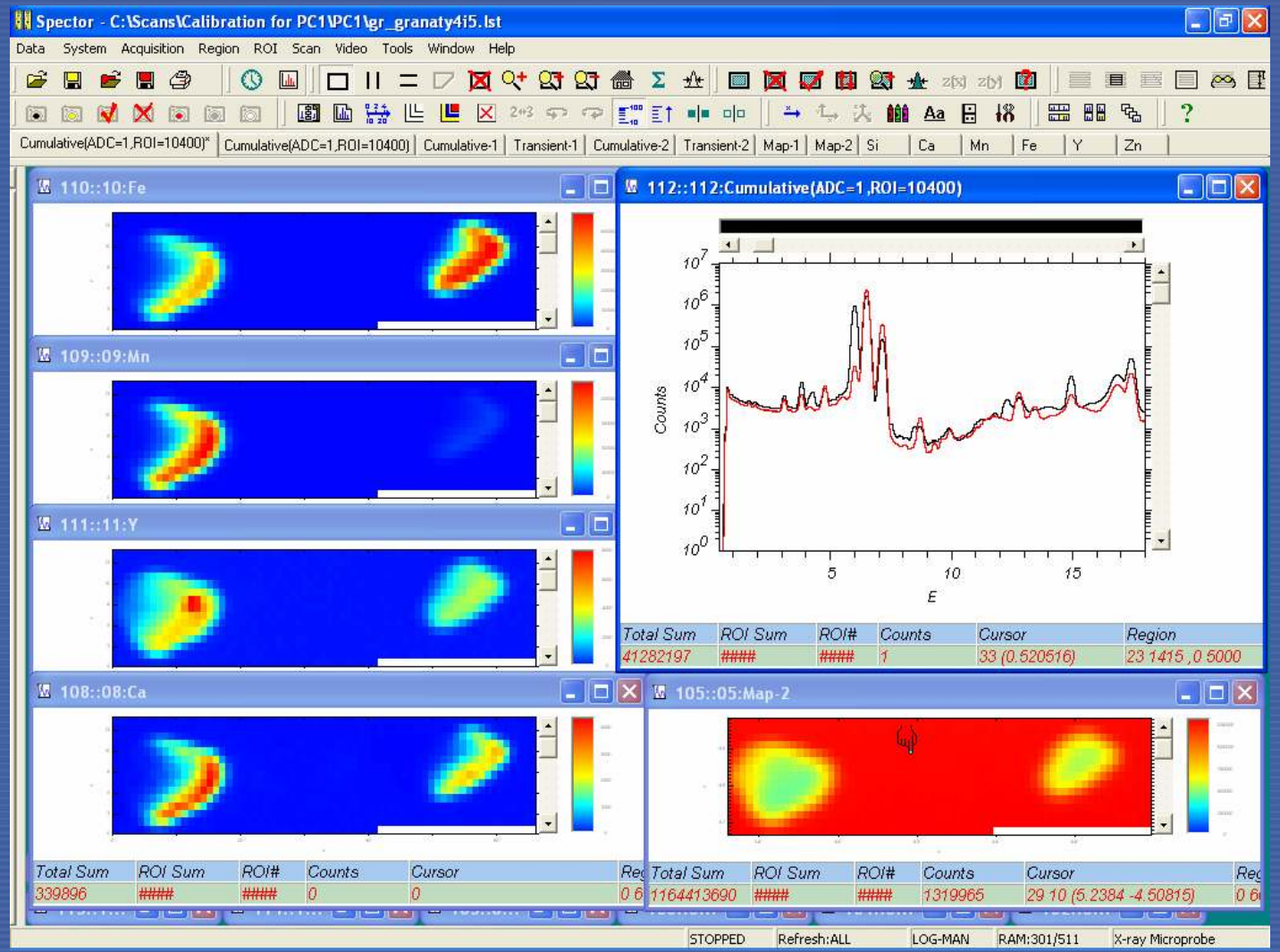

IAEA

Homogeneity testing of a candidate Reference Material

- Based of the cumulative X-ray fluorescence spectrum of the MERCK CertiPUR standard the sensitivity curve is established. The thickness of the standard residue, confirmed by the data from transmission measurements, was well within the “thin sample” approximation – the sensitivity values were calculated assuming a “thin sample” model.

- The sensitivities obtained in step 1 are used to calculate the element concentrations in the dried residue samples prepared from the candidate RM. The obtained concentrations are corrected for absorption, using the data from transmission measurements.

IAEA

Homogeneity testing of a candidate Reference Material

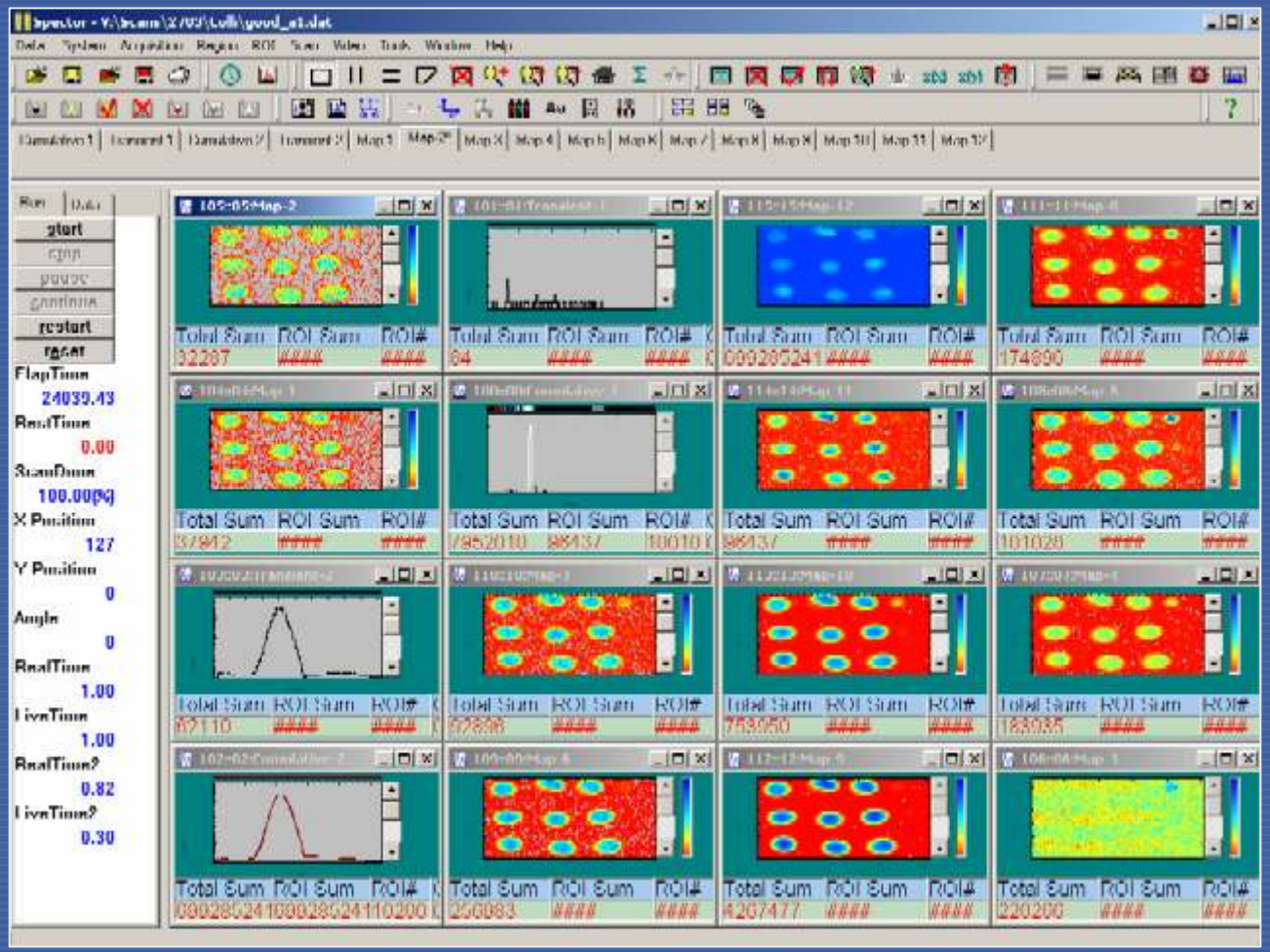

IAEA

Homogeneity testing of a candidate Reference Material

- Determination of the sensitivity calibration curve:

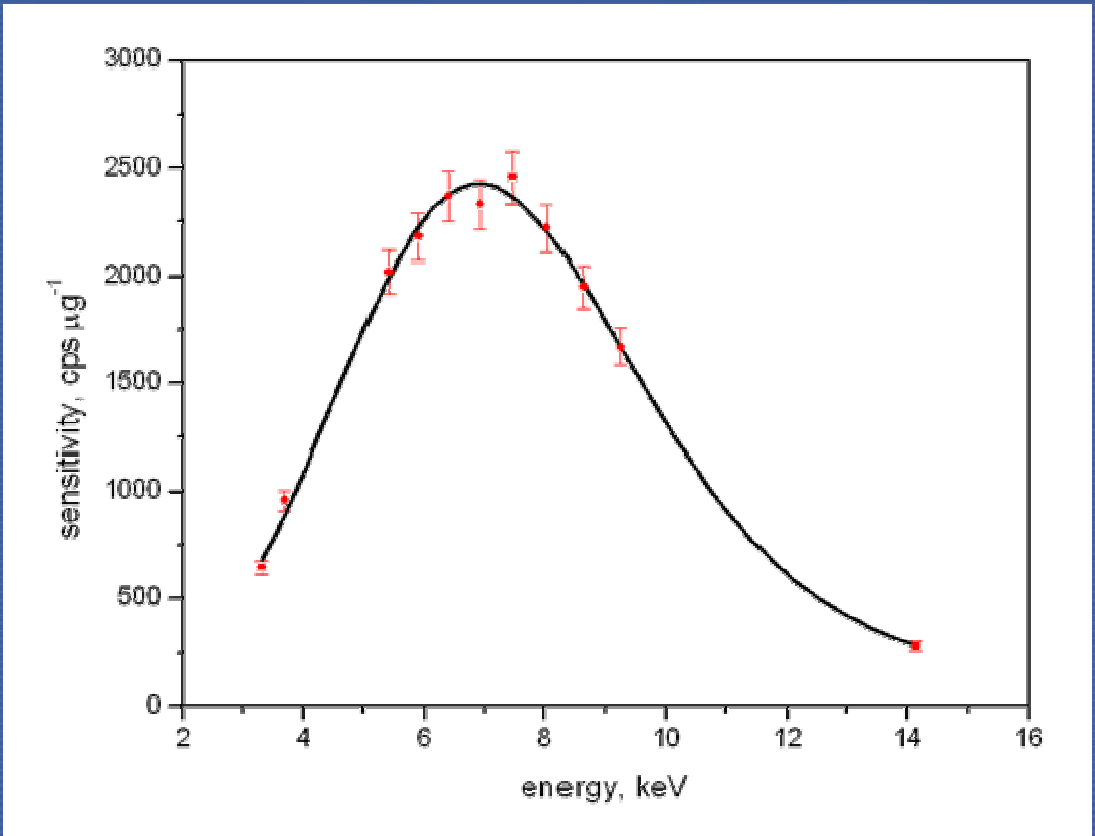

$$(I)_S = S(Z)m$$

$$(I)_x \approx S(Z_x)m_x F(E_{eff}, E_x)$$

$$c_x = \frac{m_x}{m_u}$$

IAEA

Homogeneity testing of a candidate Reference Material

$$F(E_{eff}, E_x) = \frac{1 - \exp\{-((\mu\rho d)_{eff} + (\mu\rho d)_x)\}}{(\mu\rho d)_{eff} + (\mu\rho d)_x}$$

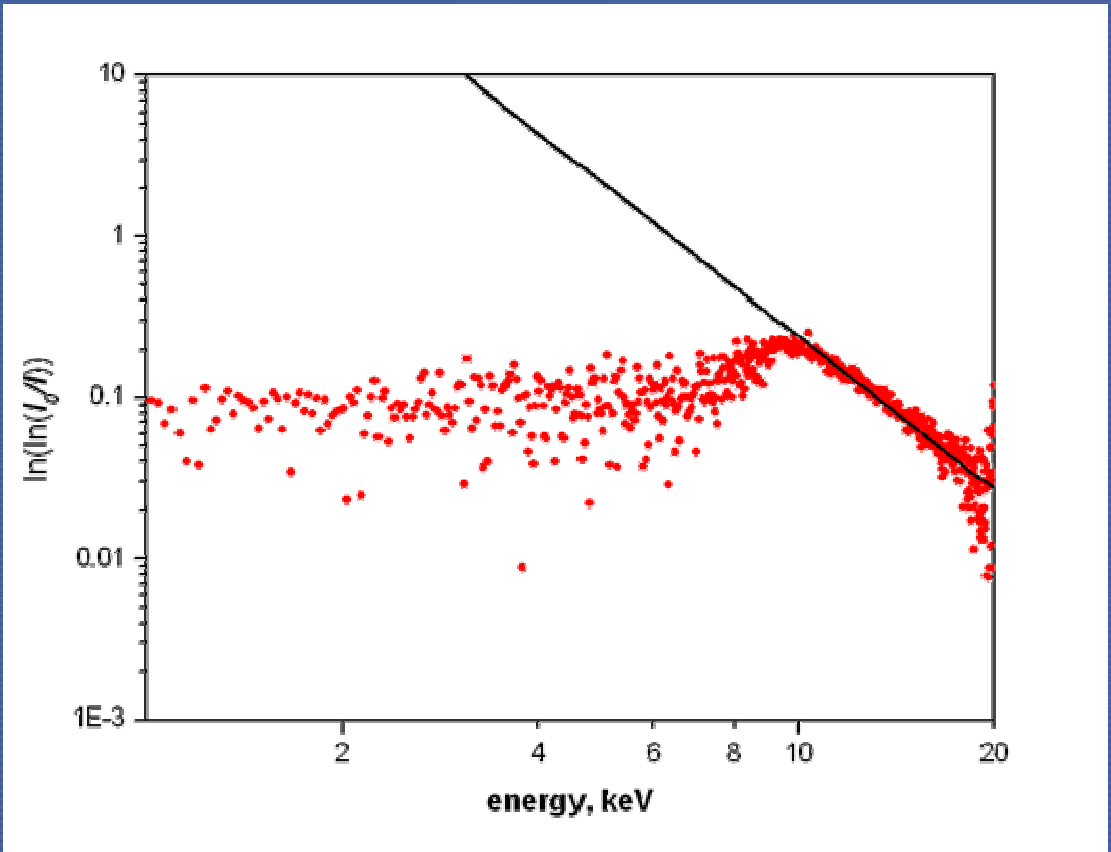

- Estimation of the absorption correction factor

IAEA

Homogeneity testing of a candidate Reference Material

	Known Concentration	Determined Concentration
Ti	0.884% (0.082)	0.82 % (0.055)
Cr	352 ppm (22)	288 ppm (50)
Mn	1757 ppm (58)	1670 ppm (90)
Fe	7.91 % (0.24)	6.8 % (0.3)

IAEA

CT Principle – Parallel Beam Projections

2D/3D CT scan (absorption and/or fluorescence)

“Replay” of the scan with optimised ROI’s, export of the sinogram data

Absorption correction of the fluorescence sinograms

Construction of interpolated sinograms for 3D scans

Reconstruction of the object cross-section(s) by filtered back projection algorithm

Volumetric rendering, 3D reconstruction, 3D mapping of element distribution, volume and area measurements

IAEA

CT Principle – Parallel Beam Projections

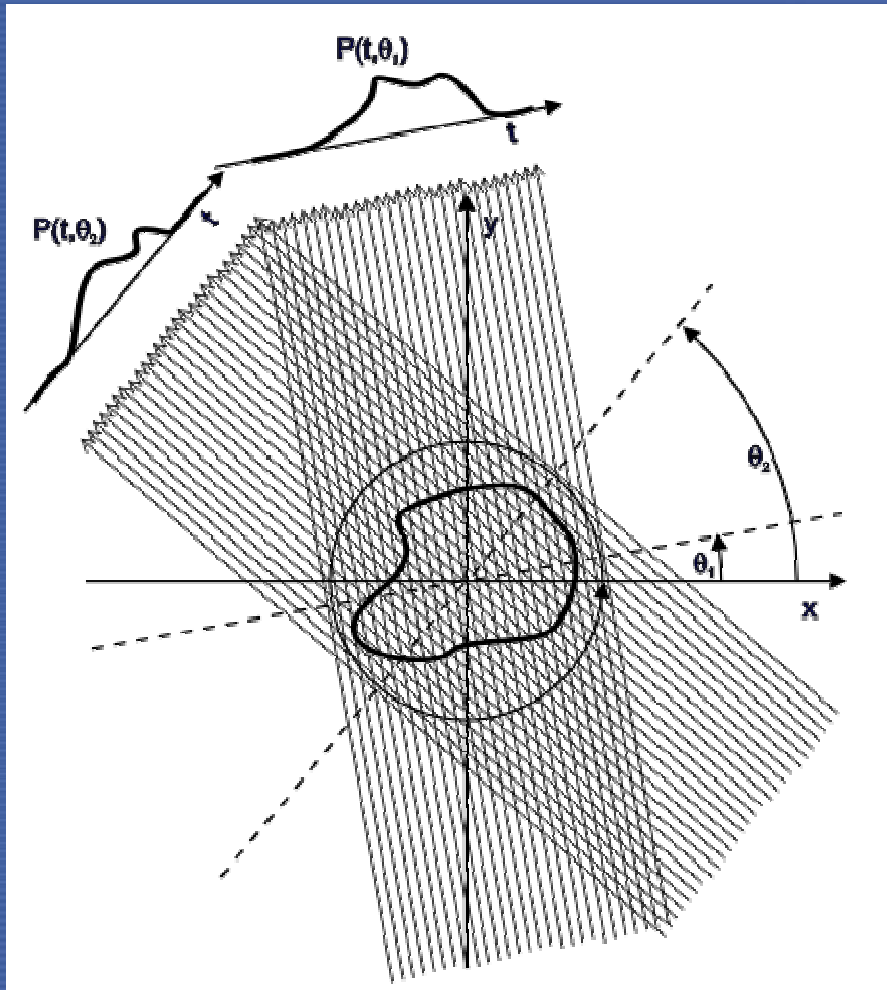

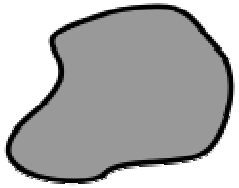

$$I(\theta,t) = I_0 e^{-\int_0^{l_{\theta,t}} \mu(x,y)\,dl}$$

$$P(\theta,t) = \ln\frac{I_0}{I(\theta,t)} = \int_0^{l_{\theta,t}} \mu(x,y)\,dl$$

$$Q(\theta,n\tau) = \tau \times IFFT\left\{\left[FFT\left(P(\theta,n\tau)\right)\right] \times \left[FFT\left(Filter(n\tau)\right)\right]\right\}$$

$$\mu(x,y) = \frac{\pi}{m}\sum_{i=1}^{m} Q(\theta_i, x\cos\theta_i + y\sin\theta_i)$$

IAEA

CT Absorption and XRF Imaging

Simultaneous X-ray absorption and X-ray fluorescence imaging in a “pencil” beam geometry

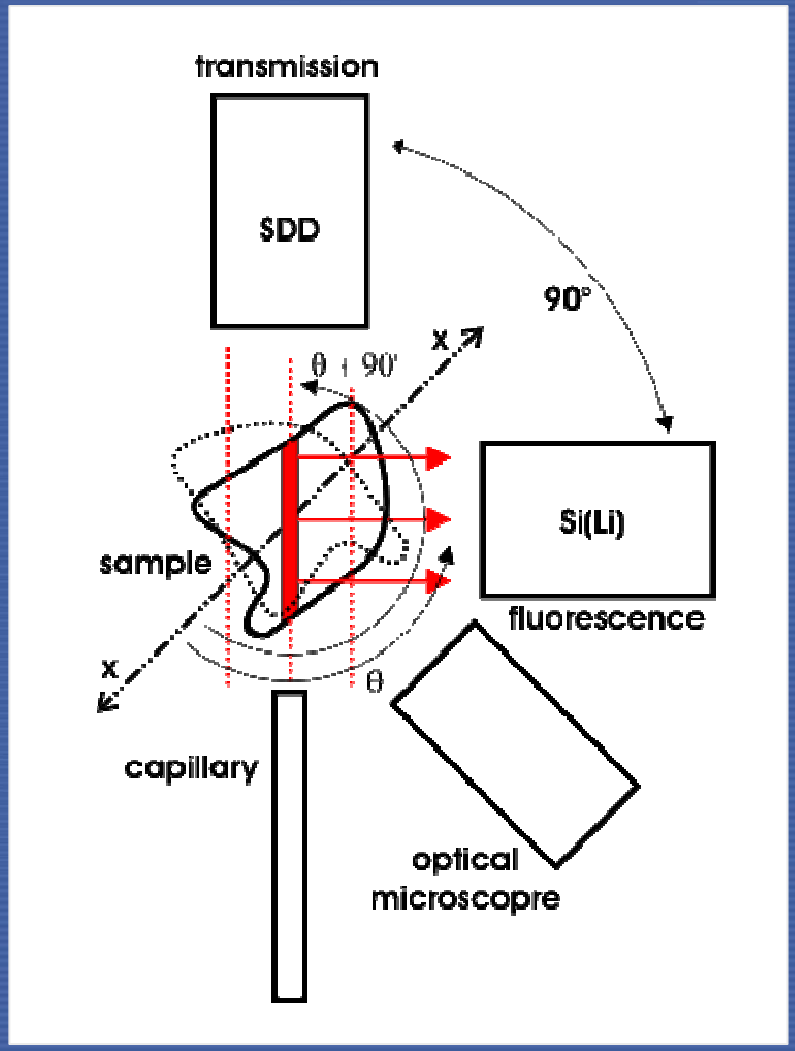

IAEA

CT Absorption and XRF Imaging

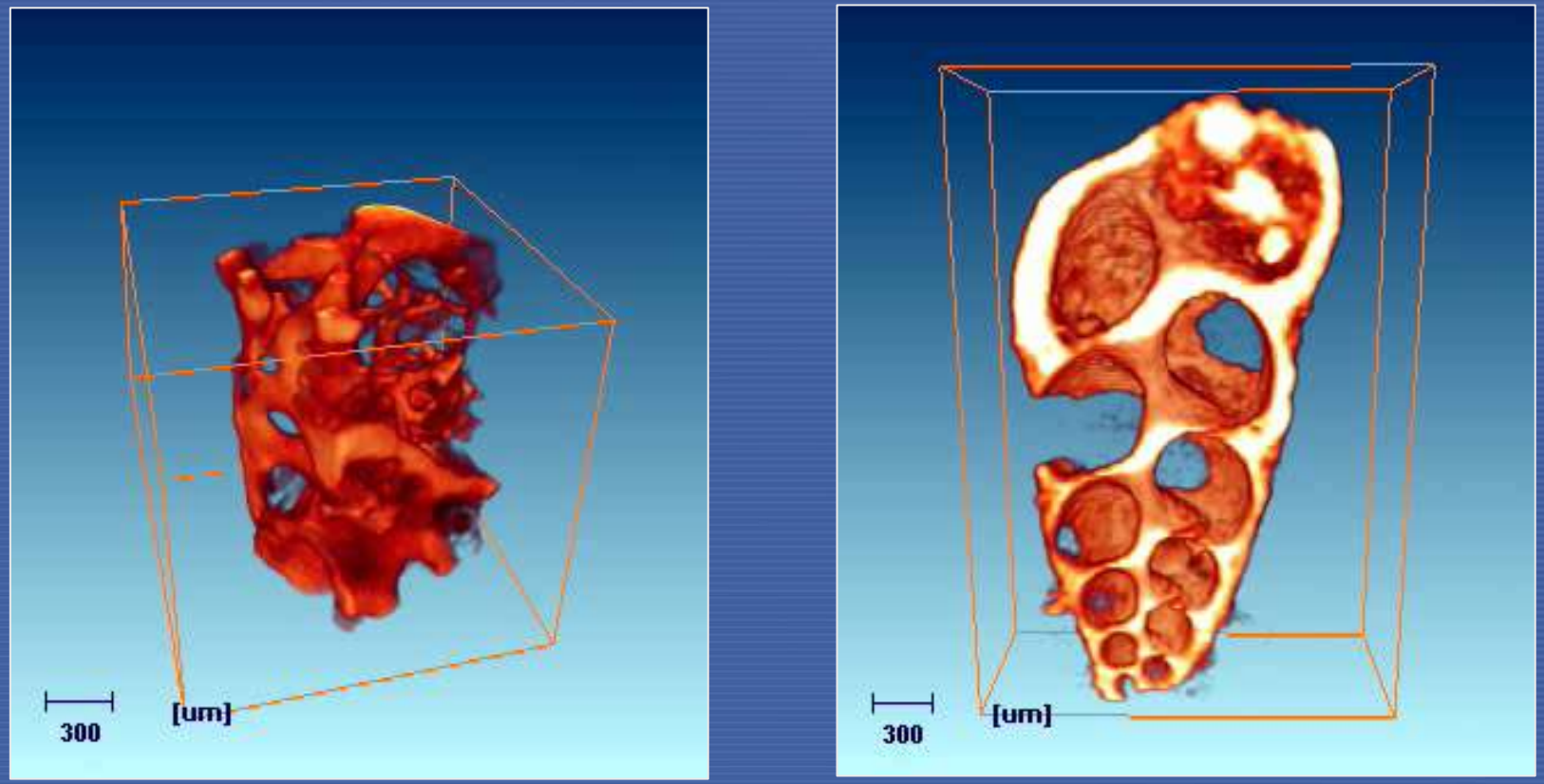

Reconstructed volumetric models of an osteoporotic bone fragment (left) and a shell fossil (right). CT absorption scan mode.

IAEA

Depleted Uranium Particle

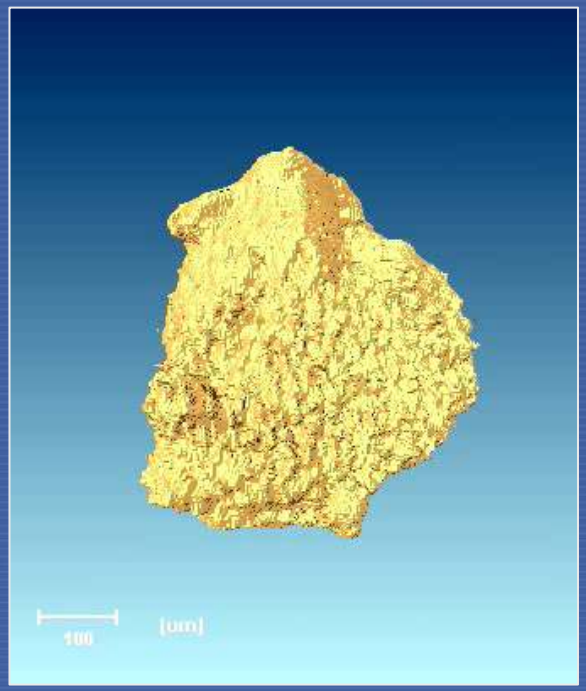

Reconstructed volumetric model (left) of a DU grain (right) obtained in absorption mode

IAEA

Depleted Uranium Particle

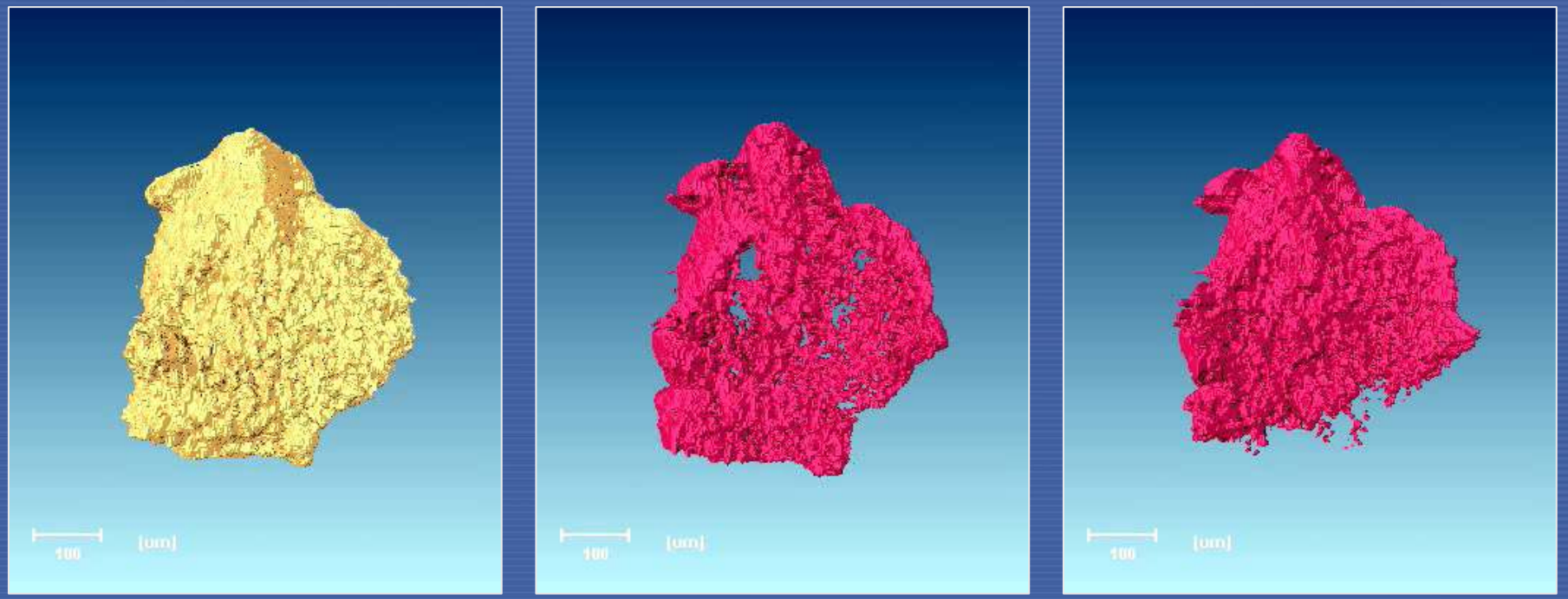

Reconstructed volumetric models of a DU grain (left to right): absorption, U-La not corrected for absorption and U-La corrected

IAEA

Depth profiling of element distribution with confocal setup

a) – g) distributions of the intensities of scatter peaks, K-Ka, Ca-Ka, Mn-Ka, Fe-Ka, Zn-Ka, and U-La obtained from cross-sectional confocal X-ray fluorescence scan through the root tip. Scan parameters: step size dx = 22.124 μm, dy = 20.000 μm, scan size 19x21 pixels, spectra acquisition time per pixel = 500s for "live pixels", 1 s for others, spatial resolution of the confocal setup FWHM = 60 μm, Mo-anode X-ray tube operated at 45kV/40 mA; h) cumulative X-ray spectrum (sum of all individual pixel spectra) collected during the confocal scan; i) photograph of the indian mustard root.

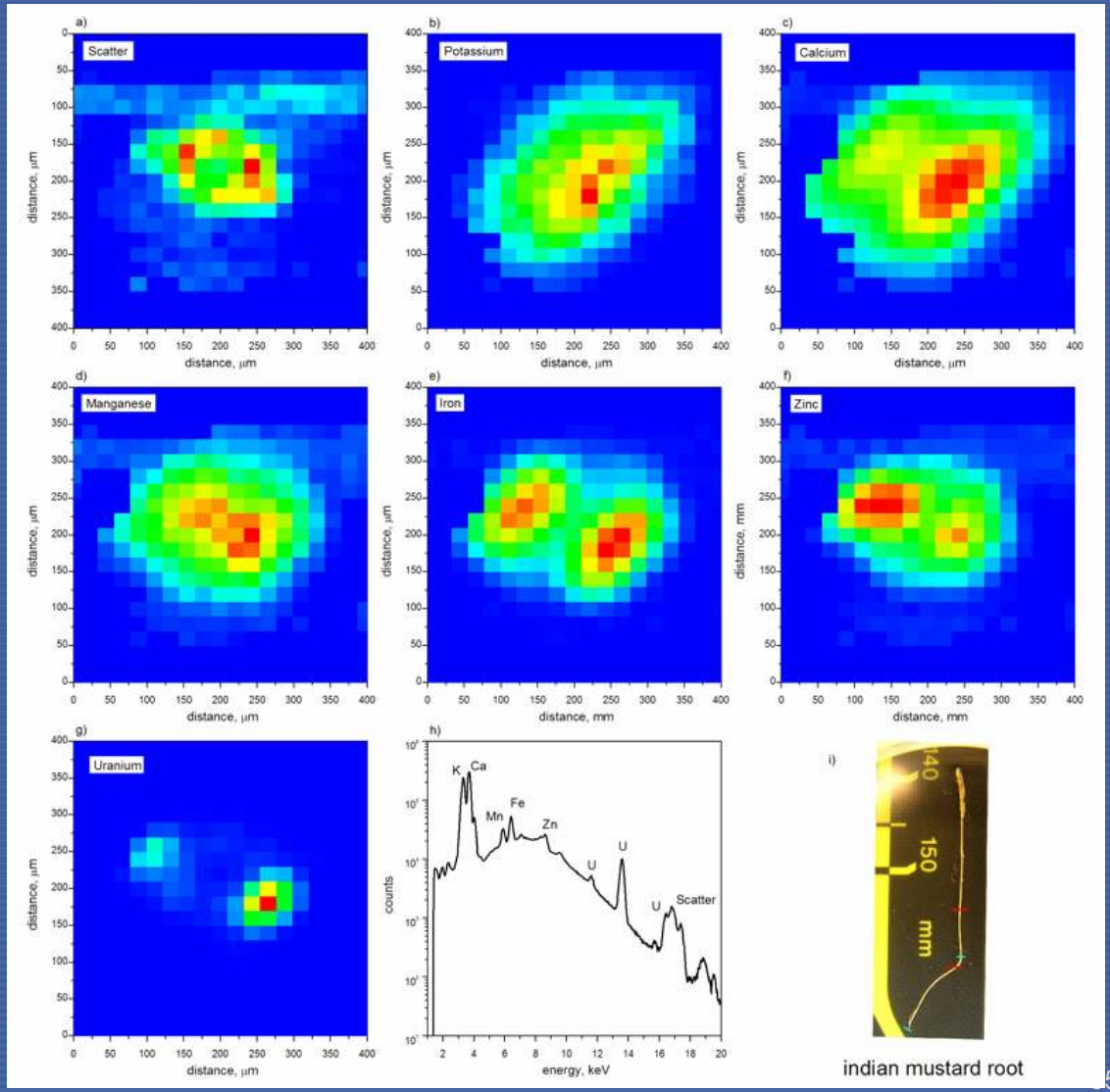

IAEA

Distribution of elements in human bone obtained by confocal scanning

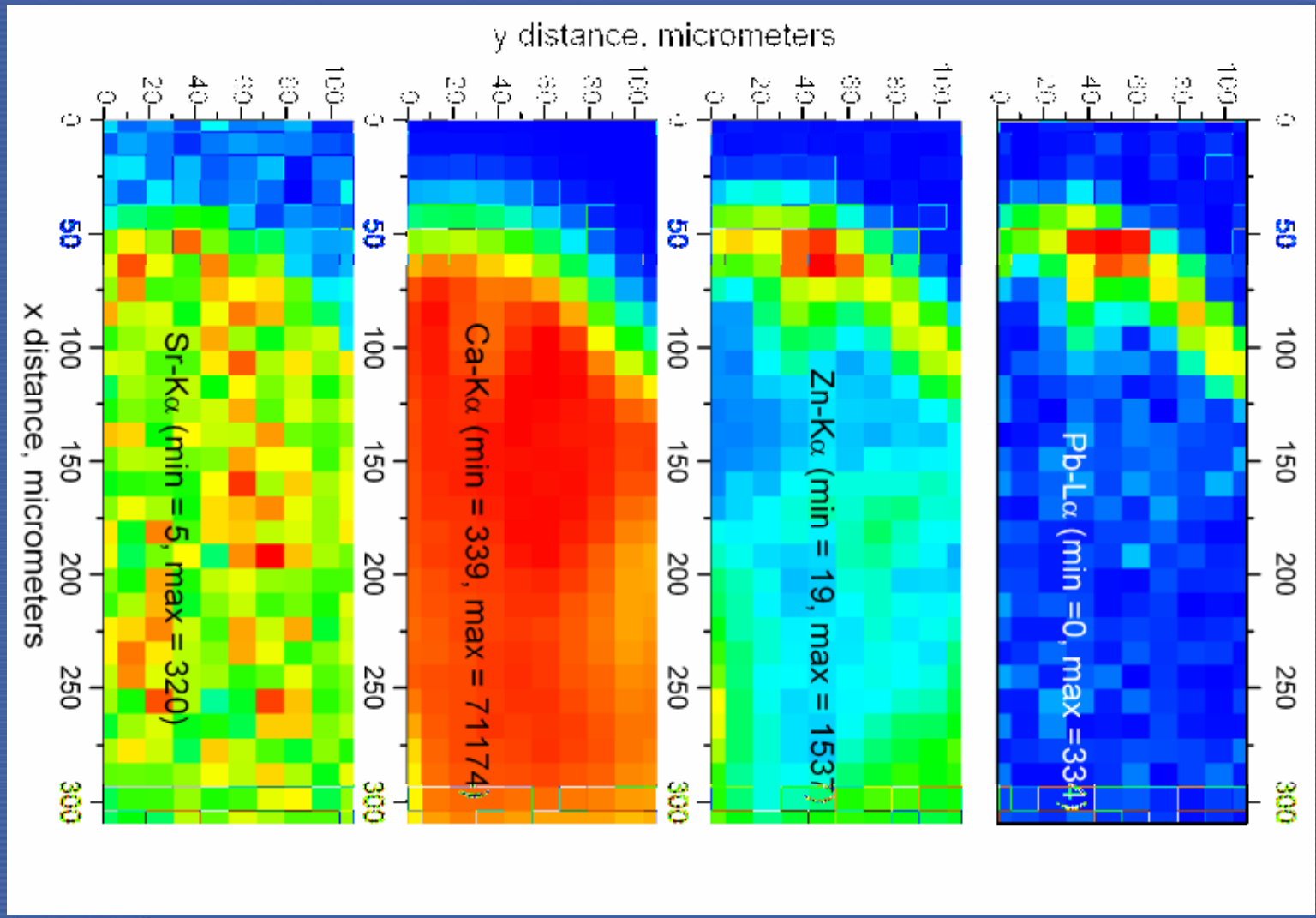

IAEA

Fe-rich plaque covering rice root

red – iron

yellow – potassium

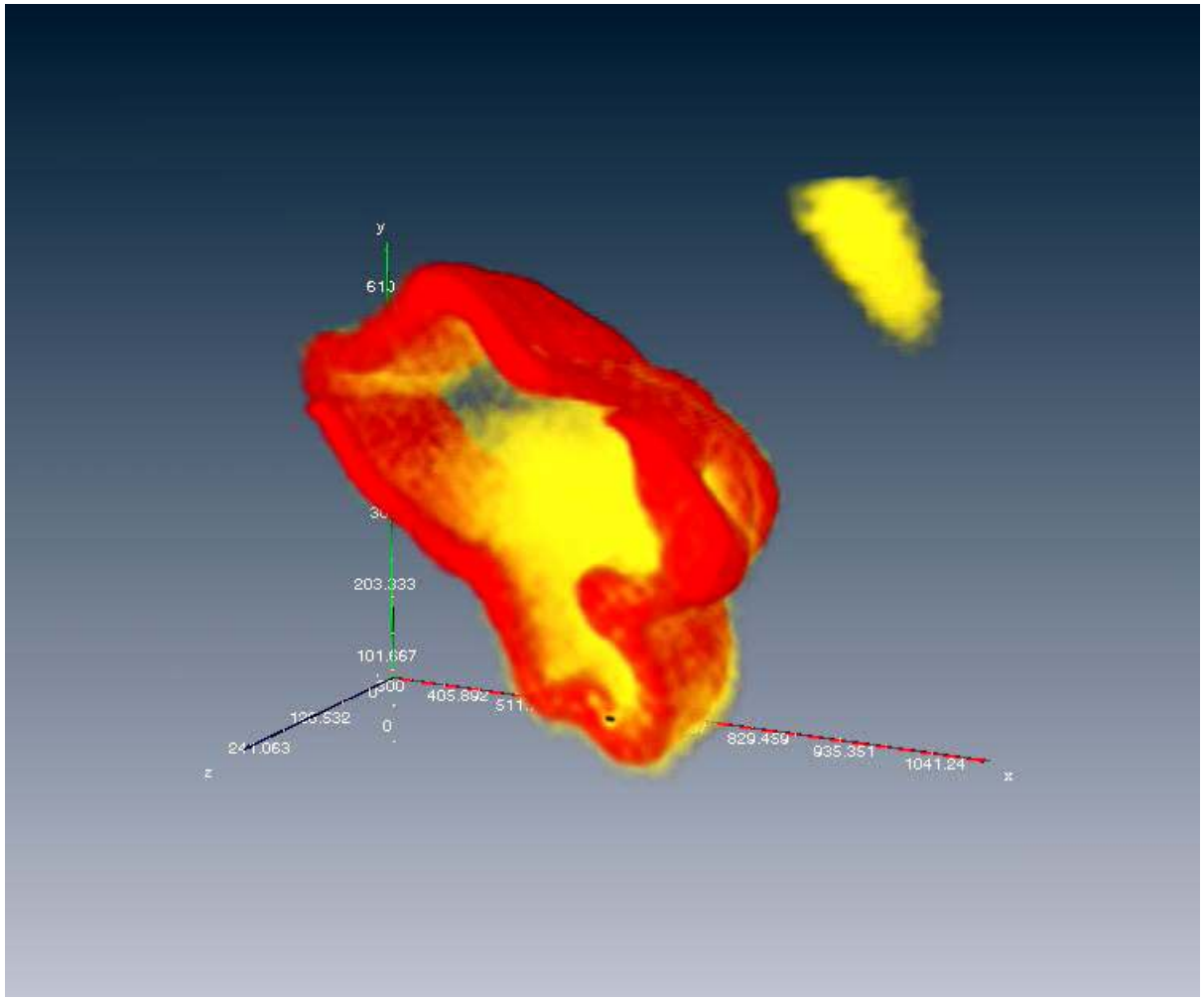

IAEA

Individual Particles

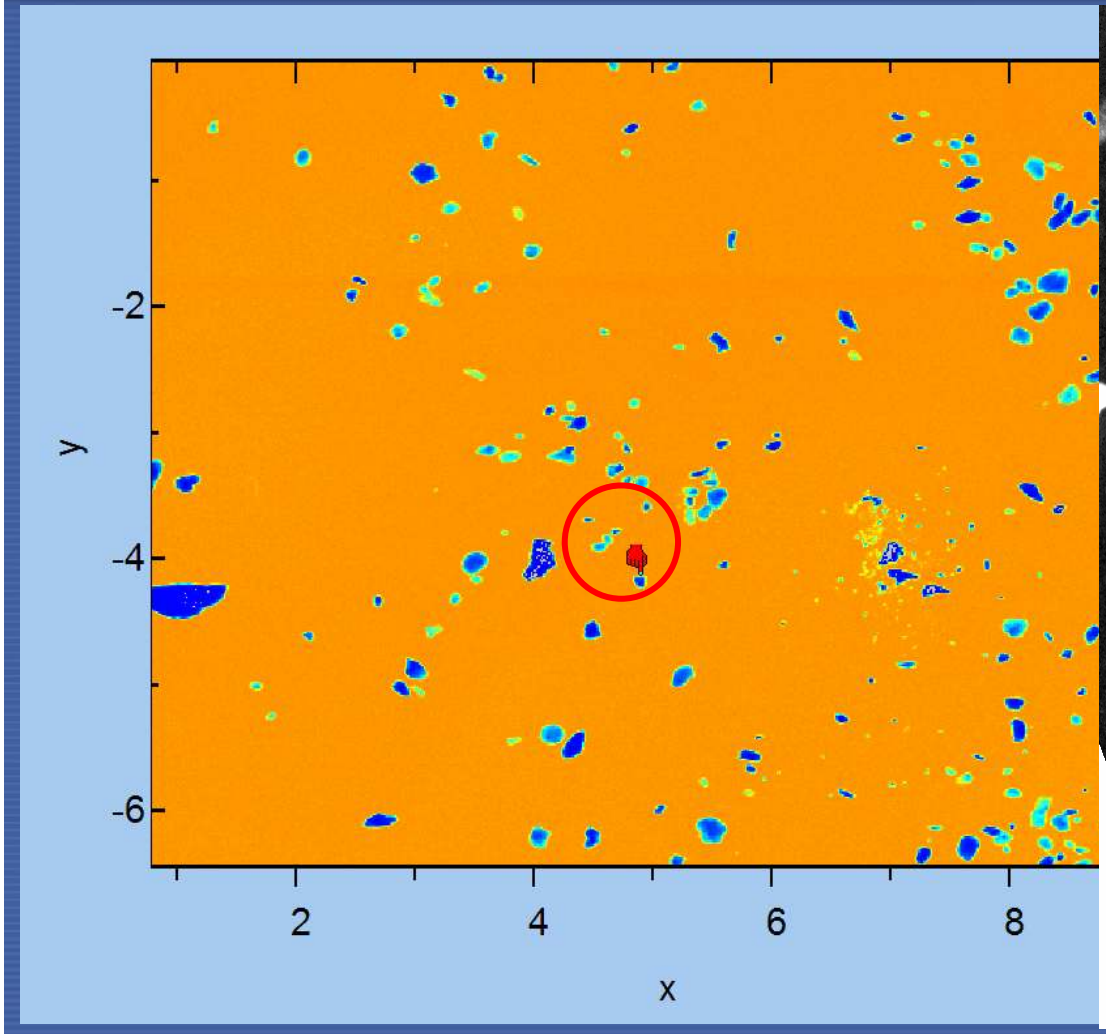

IAEA

Individual Particles

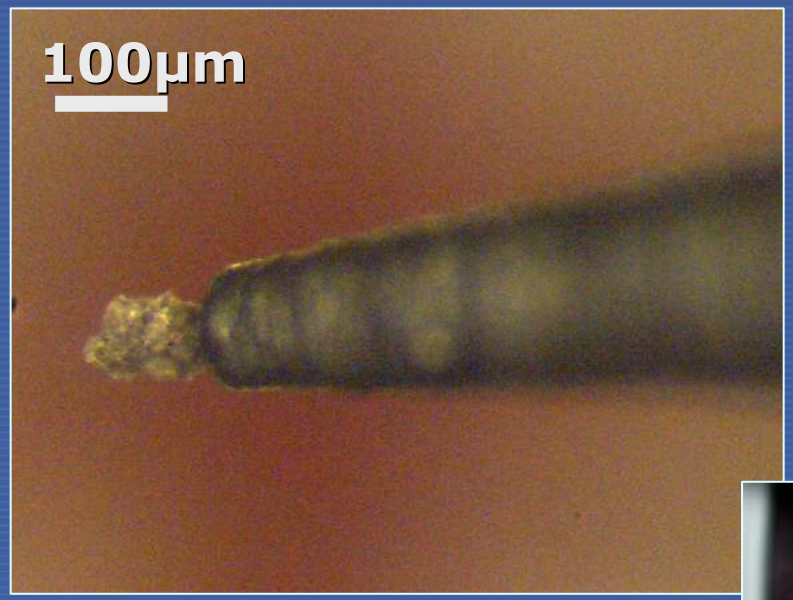

DU particle from a contaminated soil, loaded on a sharpened graphite needle

Loading the needle with a selected POI in the µ-manipulation system

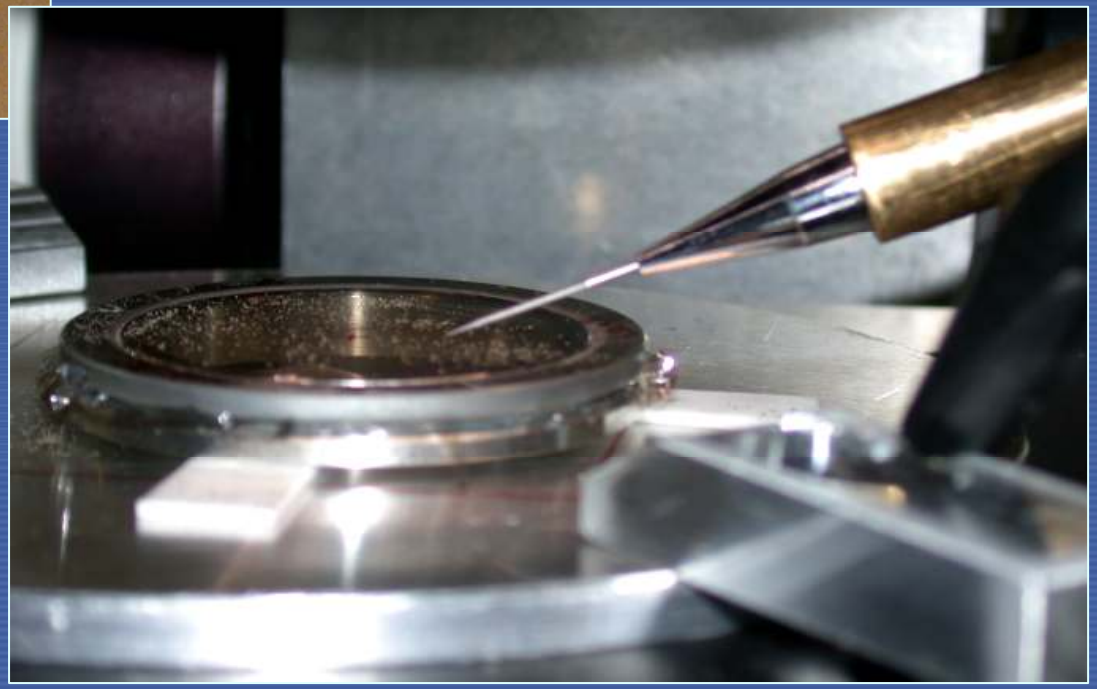

IAEA

Accelerators

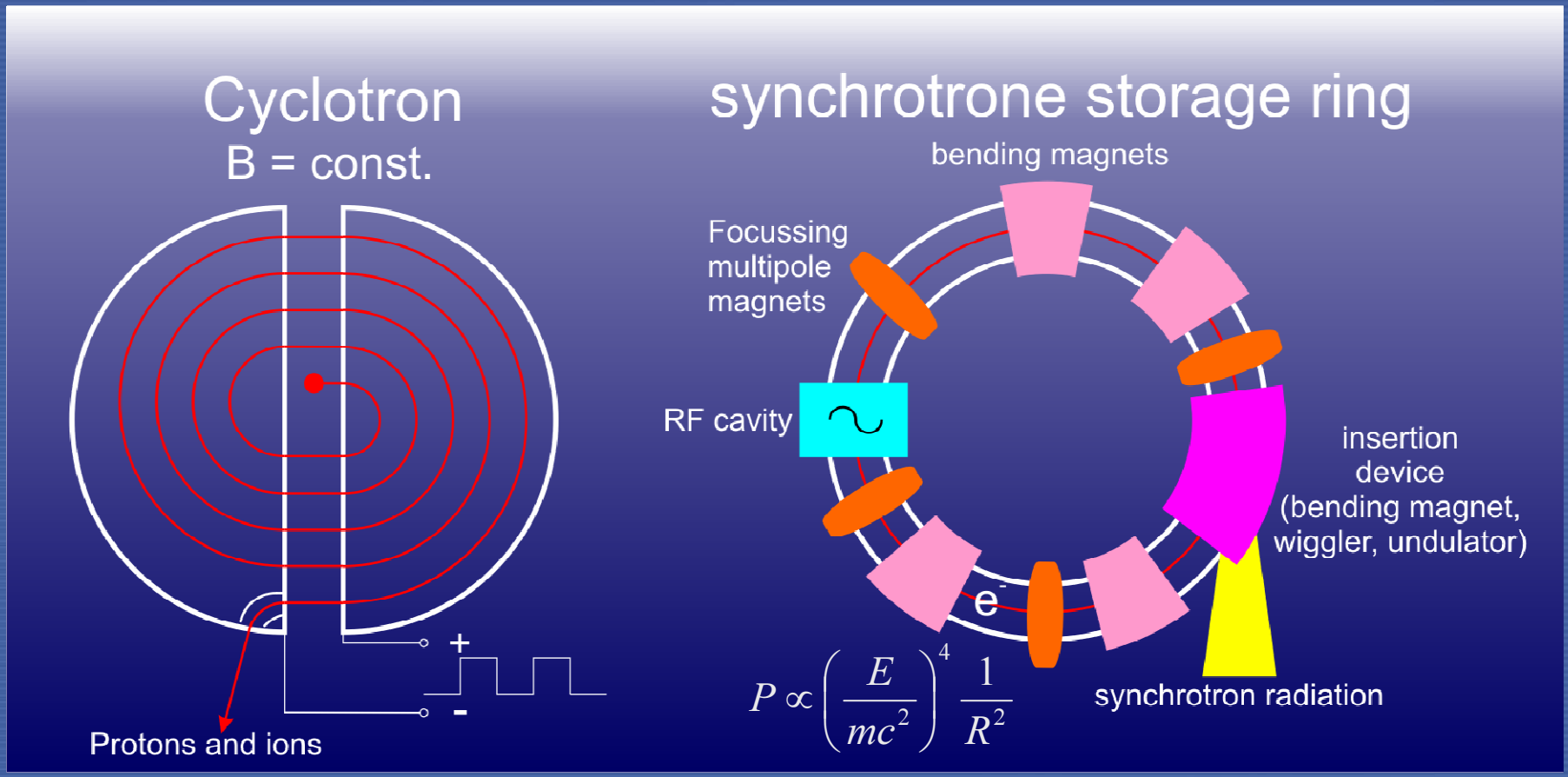

Diagrams of a cyclotron accelerator and a synchrotron storage ring

IAEA

Synchrotron light

- for a 3 GeV synchrotron storage ring: $\frac{v_e}{c} = 0.999999985$
- angular divergence (< 1 mrad): $\Delta\theta \propto \frac{1}{\gamma} = \sqrt{1 - \left(\frac{v_e}{c}\right)^2}$
- the intensity of the emitted light (radiated power) increases rapidly with the electron energy:

$$P \propto \left(\frac{E}{m_e c^2}\right)^4 \frac{1}{R^2} = (\gamma)^4 \frac{1}{R^2} = \frac{1}{\left(1 - \left(\frac{v_e}{\beta}\right)^2\right)^2} \frac{1}{R^2}$$

IAEA

Synchrotron light

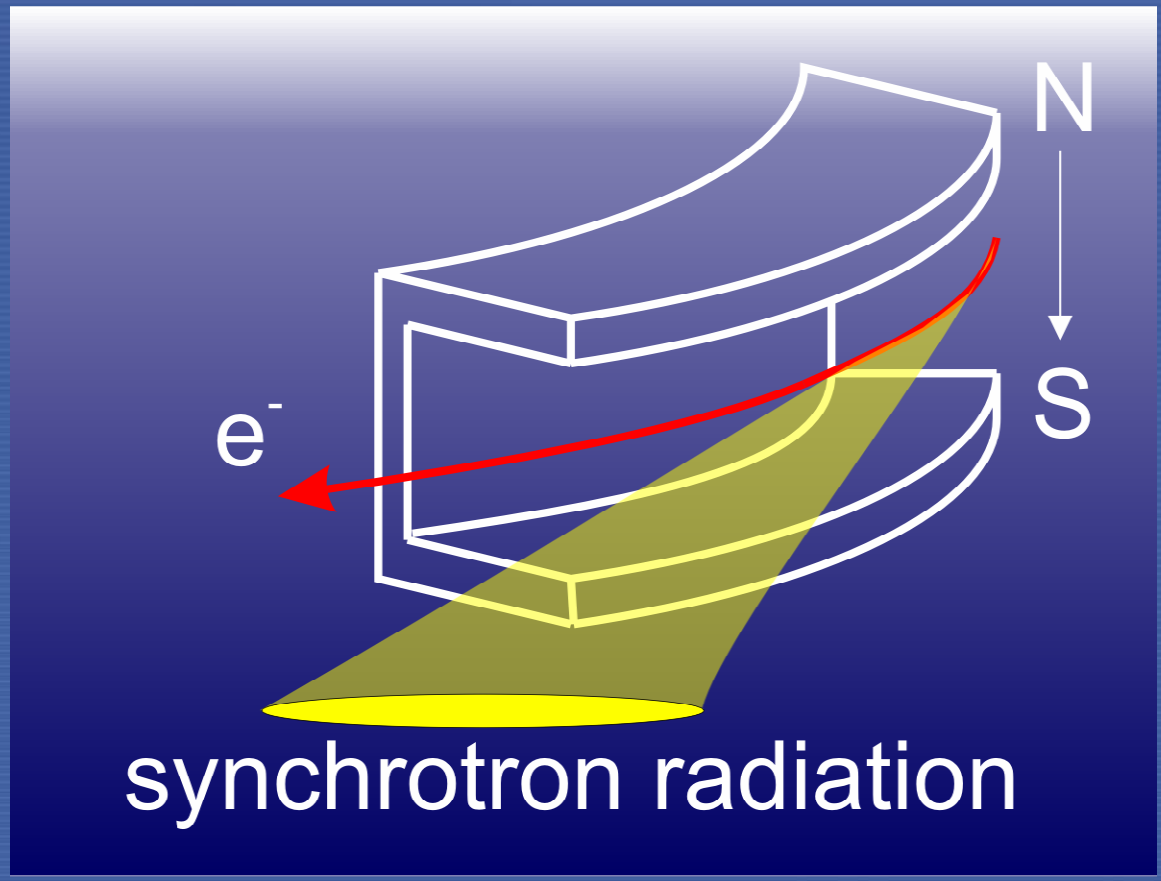

emission of synchrotron radiation by accelerated electrons in a bending magnet

IAEA

Insertion devices

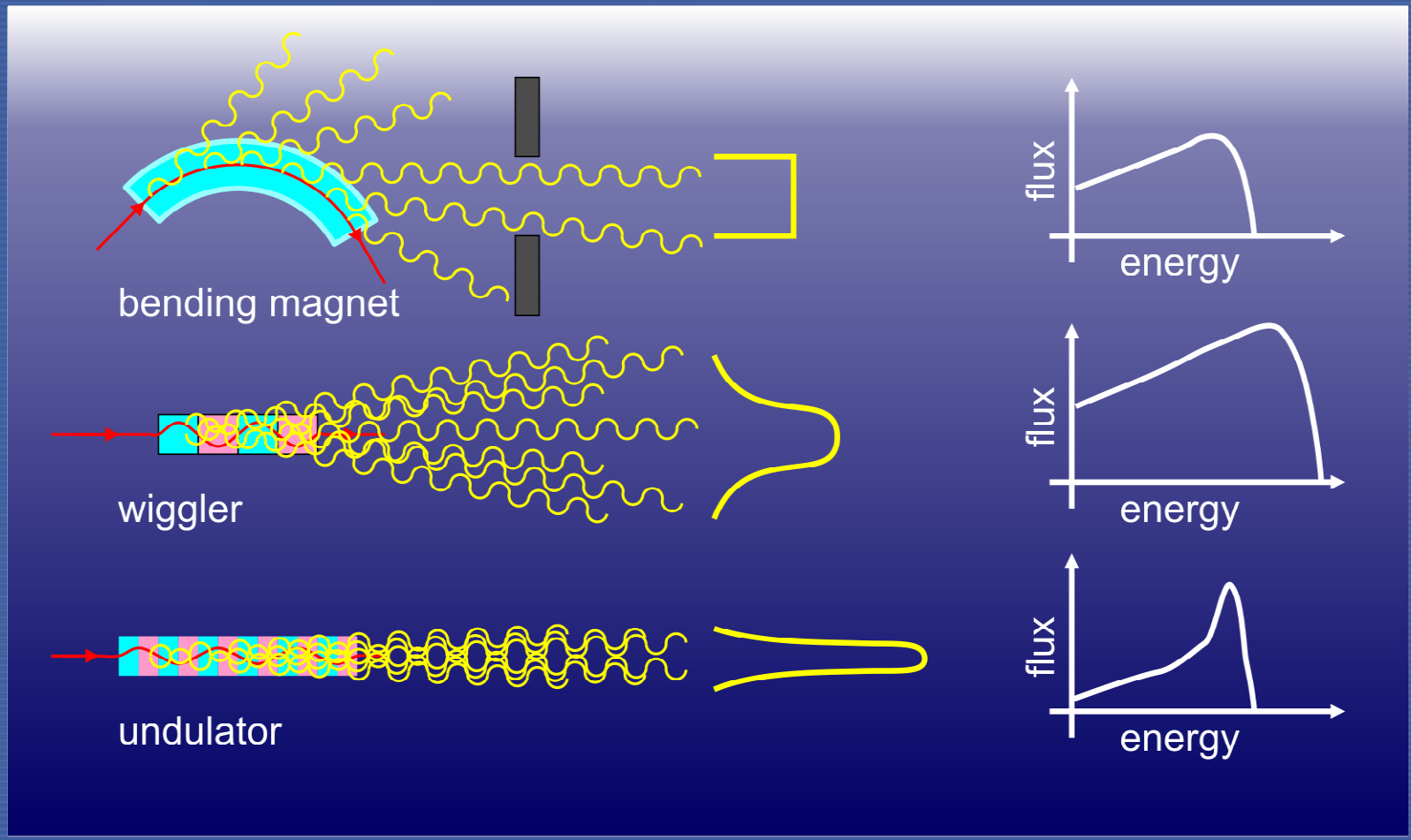

Bending magnet, wiggler, and undulator

IAEA

Angstrom Quelle Karlshure (ANKA)

The IAEA set-up at the synchrotron beamline

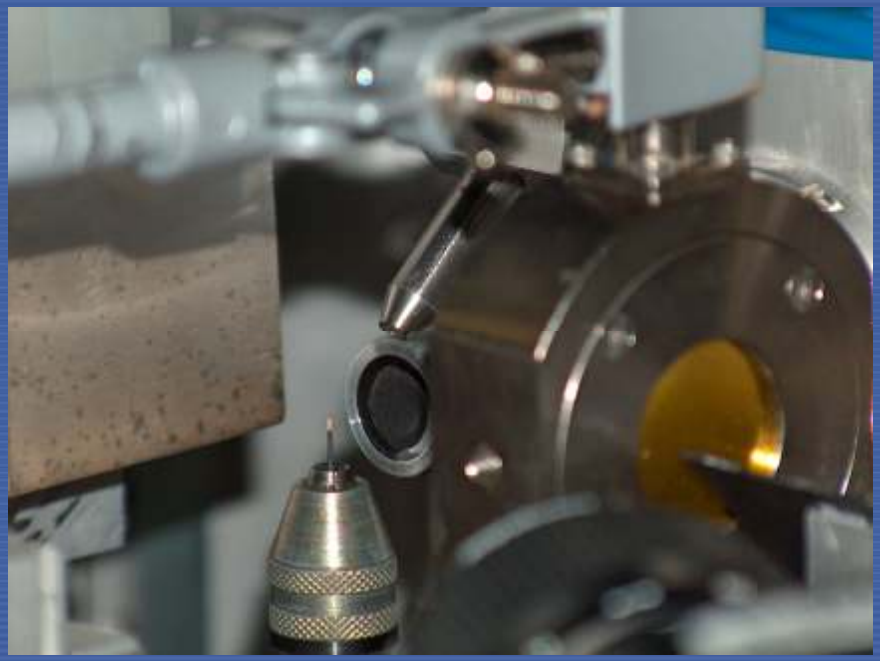

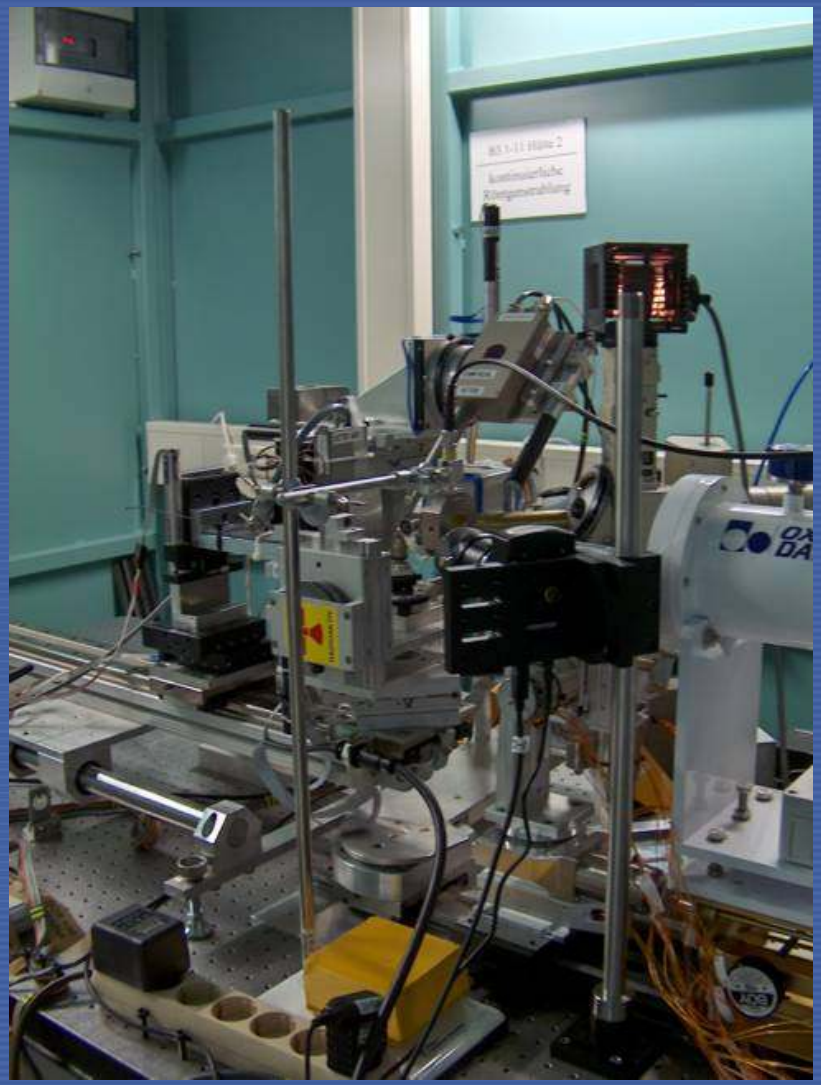

IAEA

Refractive lens - beam profile

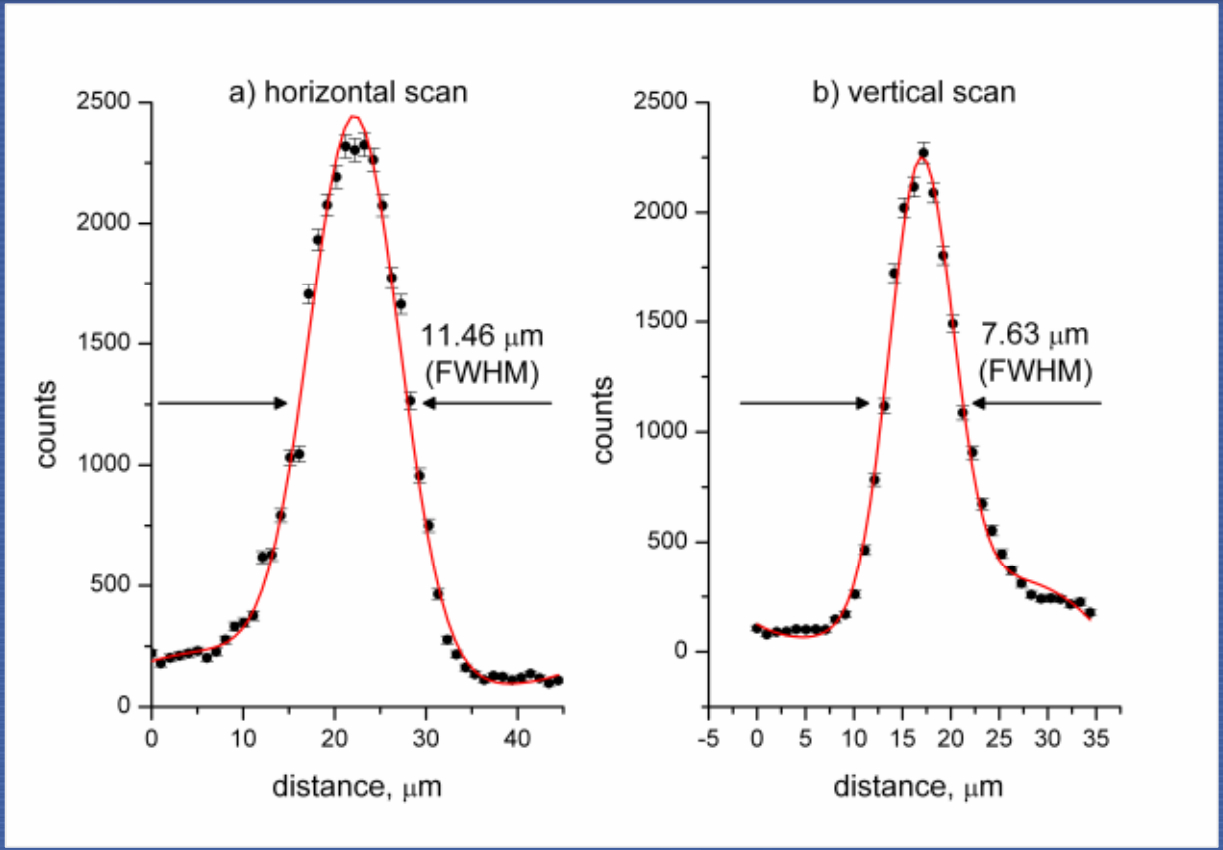

Horizontal and vertical beam dimension after focusing with compound refractive lens (CRL) optics.

IAEA

Pu/U-rich particles – X-ray tomography

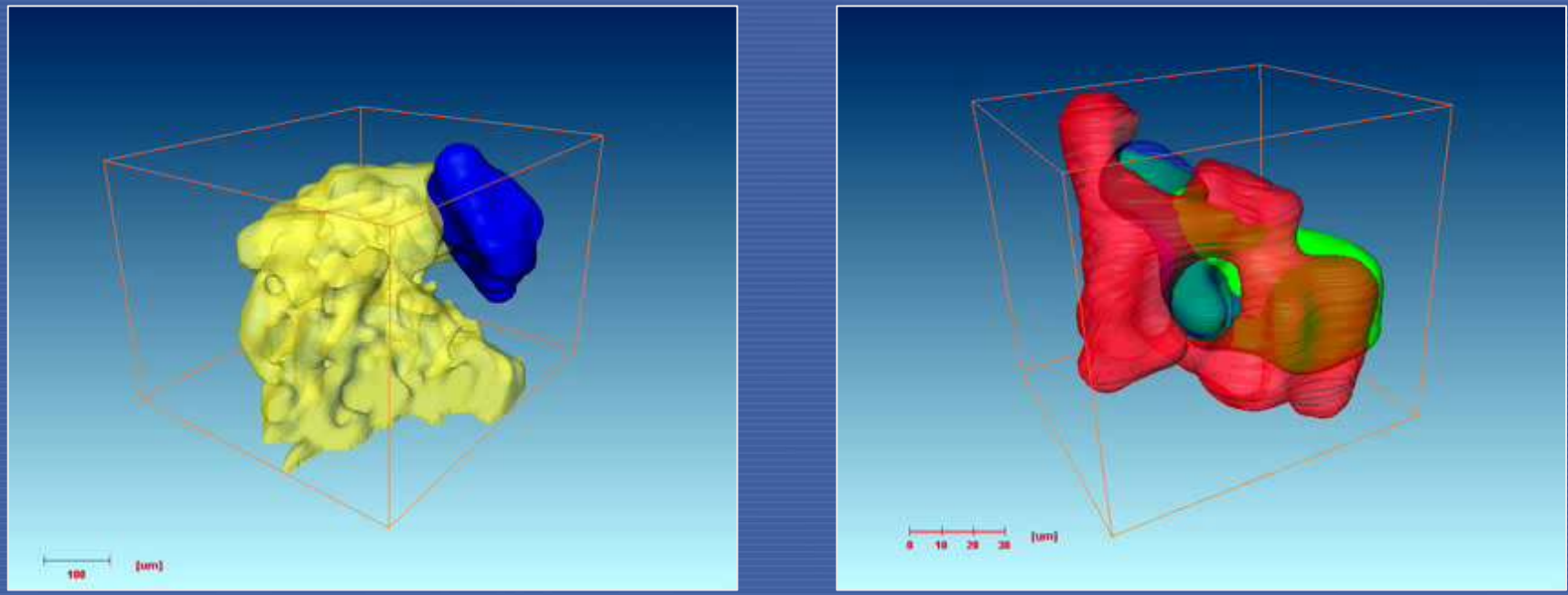

Reconstructed volumetric distributions of elements in individual “hot particles”: left - plutonium rich particle (blue) attached to a coral matrix (yellow) and right – a U/Pu rich particle (green/blue) embedded in sediment matrix (red)

IAEA

Pu/U-rich particles – X-ray tomography

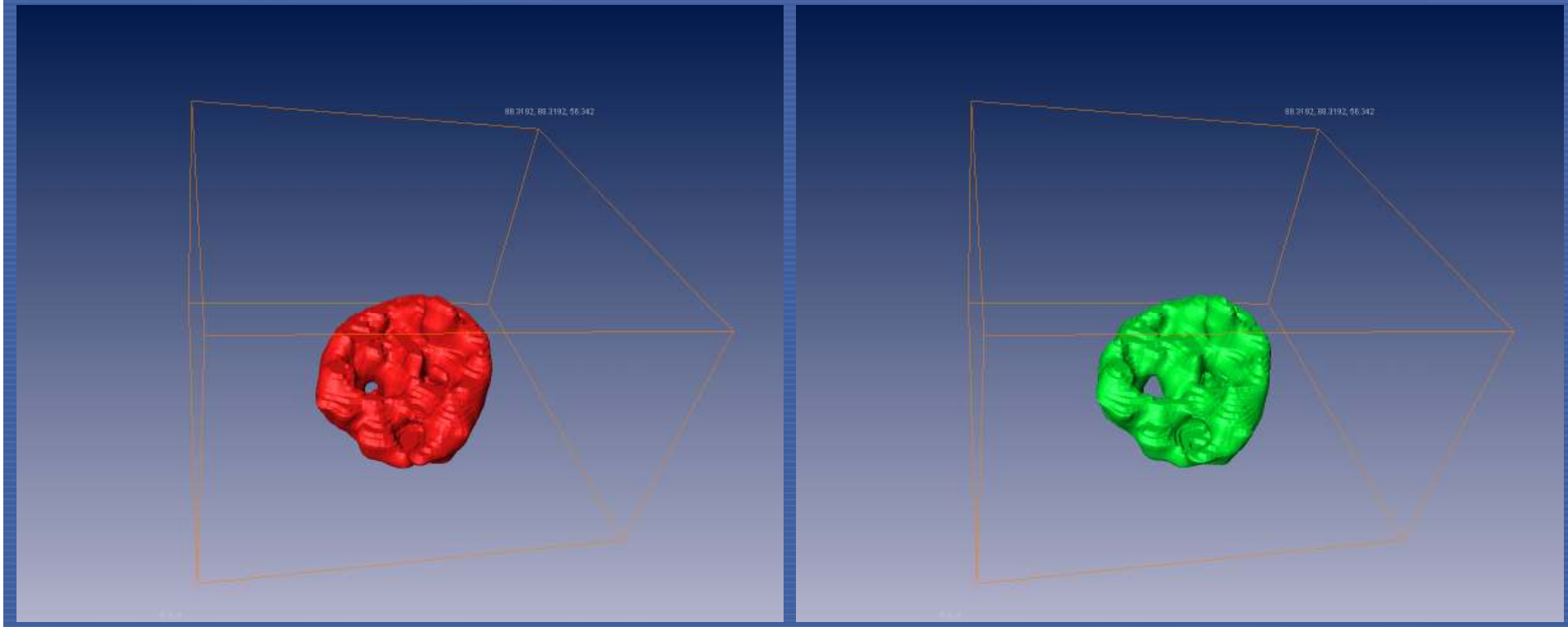

Uranium (left) and plutonium (right) distribution in a U/Pu rich particle

IAEA

Pu and U profiles

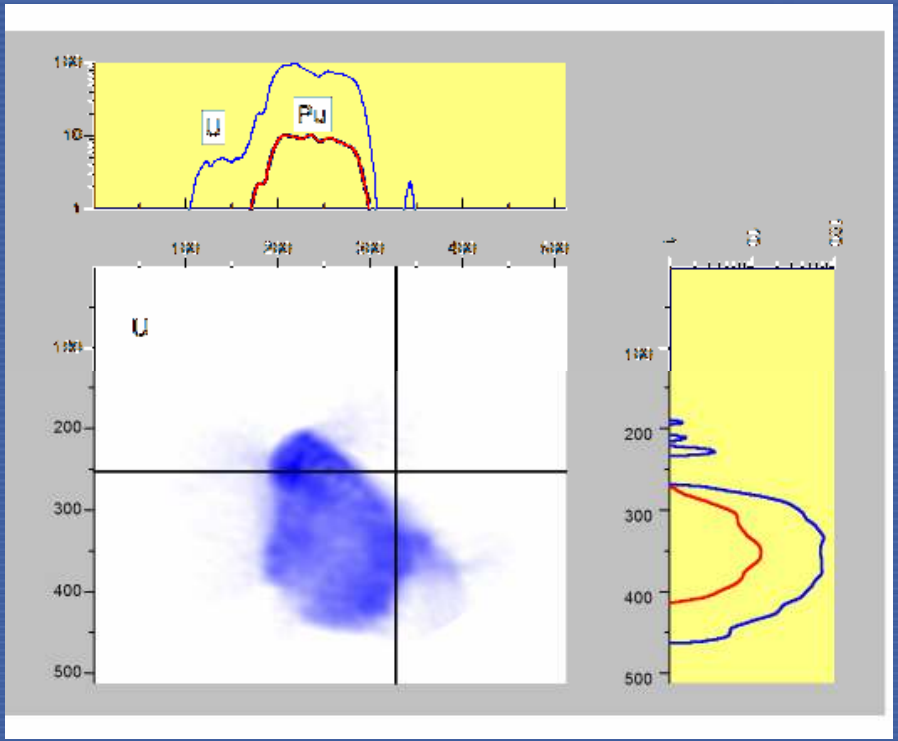

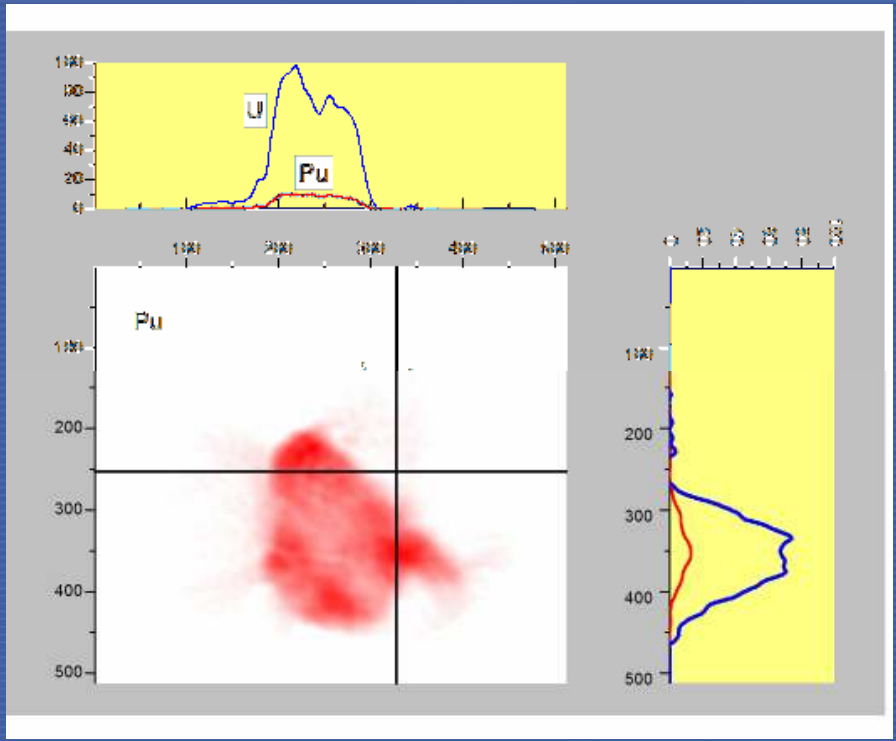

Individual particle U and Pu profiles

IAEA

Mosquito organ's imaging – possible?

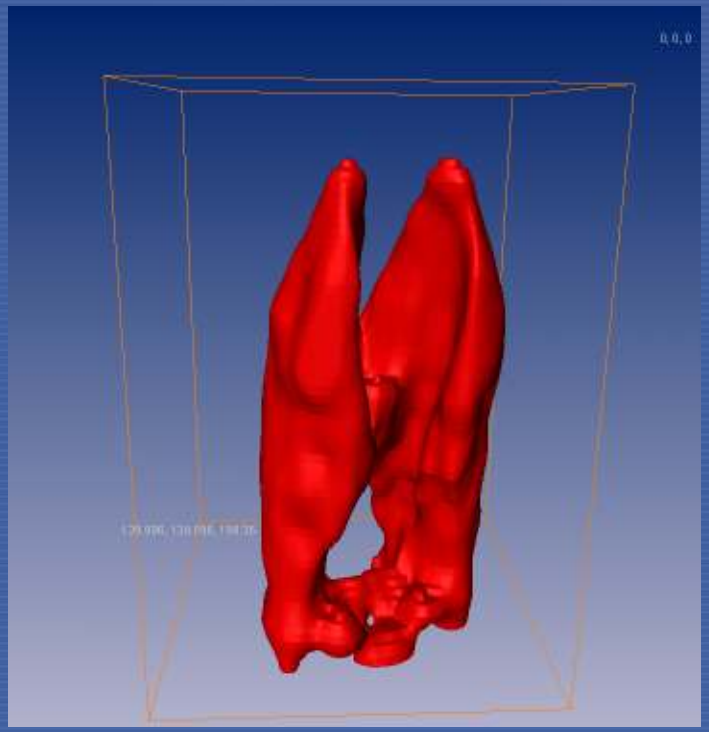

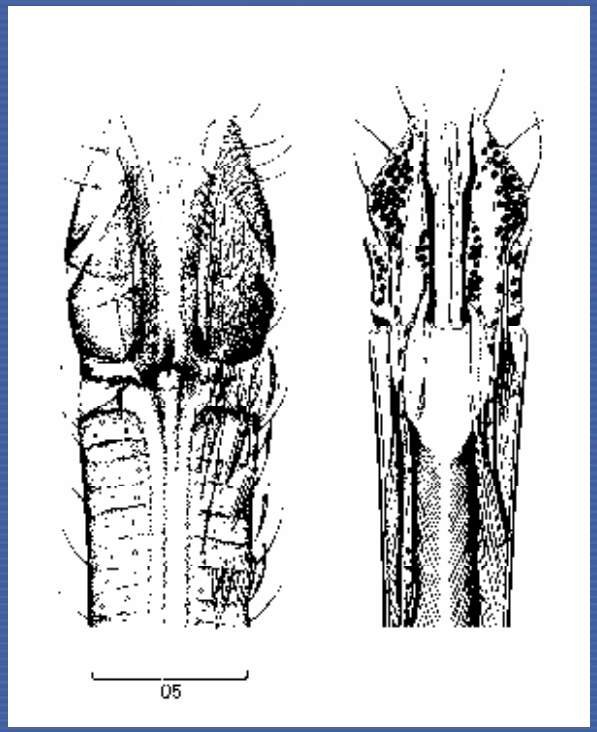

Probocsis of a female mosquito (Anopheles), tomographic reconstruction (left), anatomical drawing (right – Aedes aegypti)

IAEA

X-ray phase-contrast enhanced micro tomography

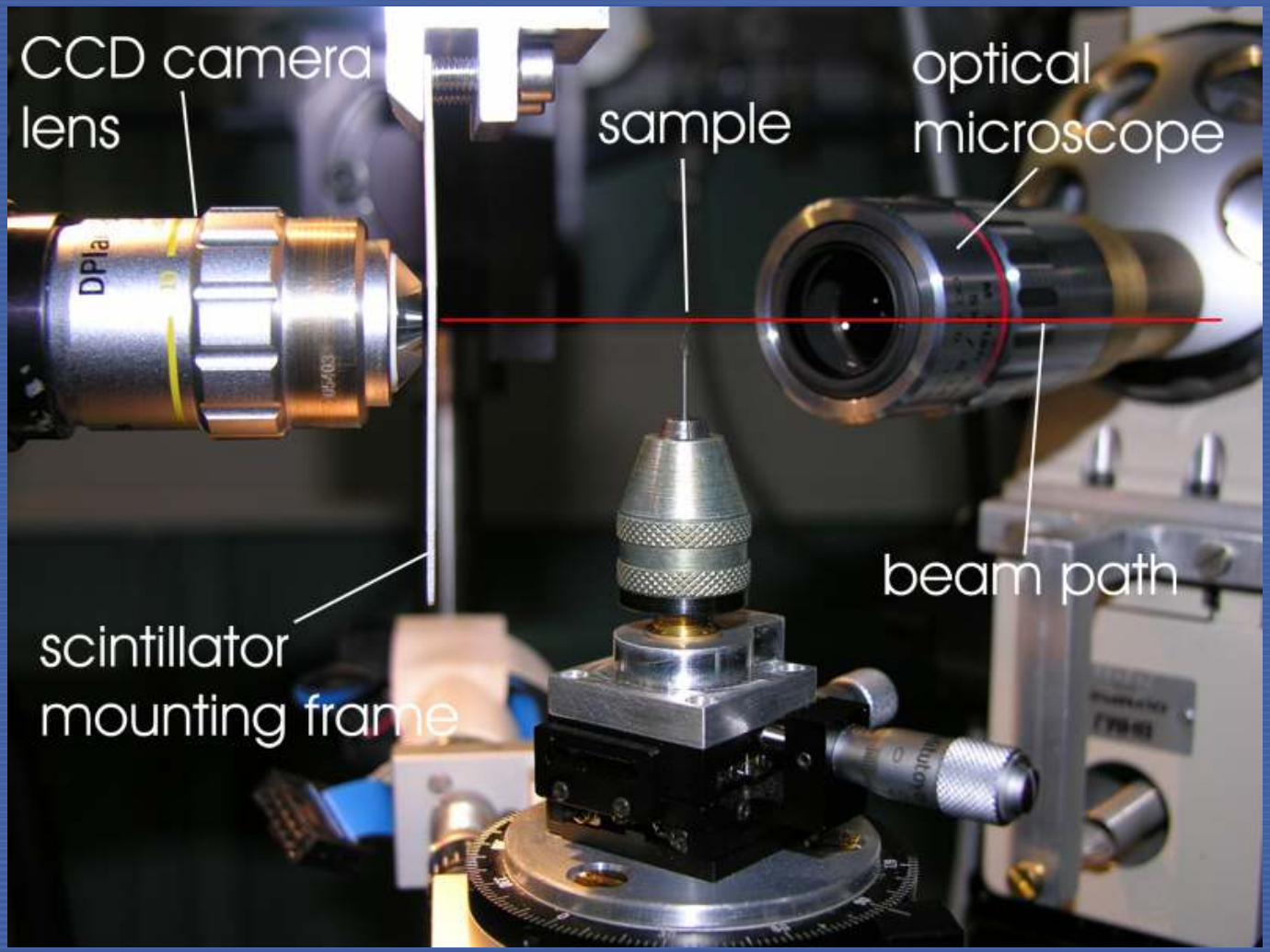

Experimental setup established at the ANKA synchrotron Fluo-Top beam line for investigating the morphology of malaria transmitting mosquitoes

IAEA

X-ray phase-contrast enhanced micro tomography

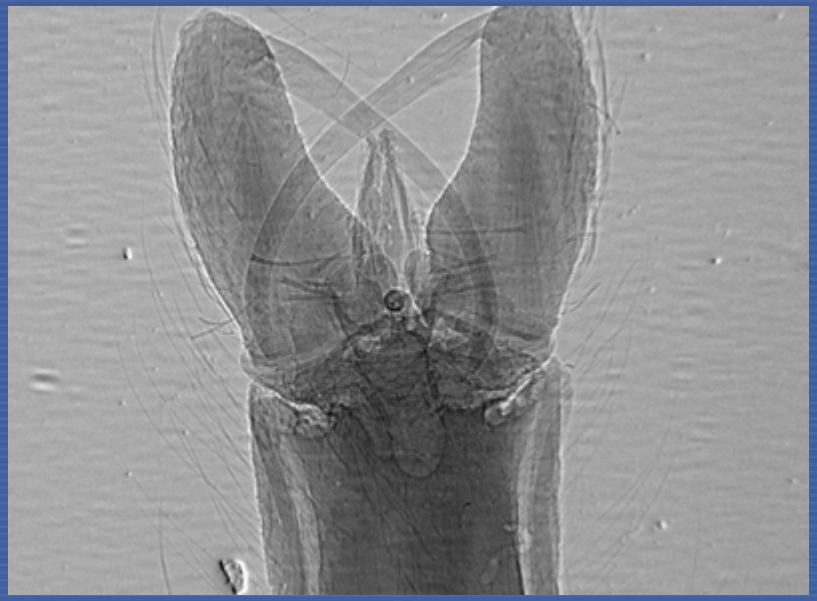

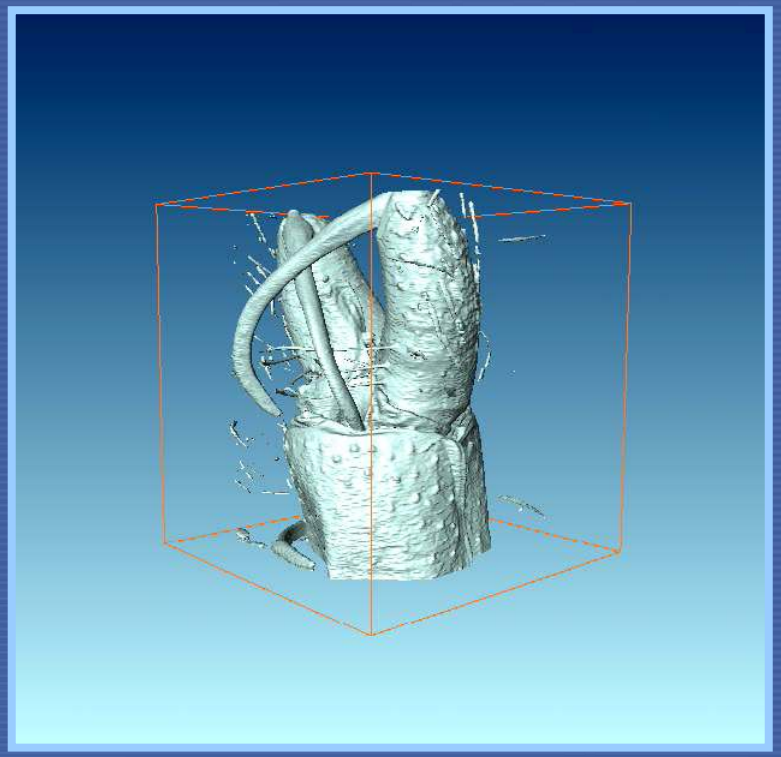

Left: single X-ray phase-contrast enhanced projection image of an abdomen of irradiated male mosquito; right: reconstructed volumetric model through the mosquito abdomen

IAEA

Phase-contrast X-ray imaging of live specimens

IAEA

Summary and conclusions

- X-ray tube based micro-analytical techniques are well suited for characterization of minute samples, and heterogeneous objects.
- Quantitative analysis is possible however much more difficult as compared to the analysis of bulk samples.
- The micro-beam X-ray techniques provide additional information about the microscopic structure of bulk material.
- When combined with synchrotron radiation very low amount of substance can be detected, coherent beam allows performing phase-contrast imaging of weakly absorbing objects, e.g. tissue, biomedical samples.

Acknowledgements

The results presented were obtained with collaboration of many people :

- A. Markowicz, E. Chinea-Cano, S. Bamford, IAEA Laboratories Seibersdorf
- P. Wobrauschek, C. Streli, N. Zoeger, Vienna University of Technology, Atominstitut, Austria
- M. Eriksson, M. Betti, S. Toeroek, European Commission Joint Research Center, Institute for Transuranium Elements, Karlsruhe , Germany
- R. Simon, S. Staub, T. Weitkamp, A. Rack, Forschungszentrum Karlsruhe GmbH, Institute for Synchrotron Radiation, Eggenstein-Leopoldshafen, Germany

IAEA

Thank you for your attention!

IAEA